Silica Nanoparticles for Diagnosis, Imaging and Theranostics

Rosenholm, Jessica; Näreoja, Tuomas

Published in:
Handbook of Materials for Nanomedicine

DOI:
10.1201/9781003045076

Published: 01/01/2020

Document Version
Accepted author manuscript

Document License
Publisher rights policy

Chapter X

Silica Nanoparticles for Diagnosis, Imaging and Theranostics

Jessica Rosenholm & Tuomas Näreoja
Pharmaceutical Sciences Laboratory, Åbo Akademi University, Turku, Finland; *jerosenh@abo.fi*
Karolinska Institute, Stockholm, Sweden; *tuomas.nareoja@ki.se*

Book Title
First Author & Second Author

www.panstanford.com

1.1 INTRODUCTION

Silicon (Si) is the second most abundant element in the earth's crust preceded only by oxygen, making Si the most abundant metallic element. Their combination (SiO_2) i.e. silica, makes up about 60% of the crust in the form of e.g. quartzite and sandstone [1]. These are crystalline forms of silica, whereas the amorphous form is well-known to e.g. the pharmaceutical, cosmetic and food industries since decades; where it is known to a large extent as colloidal (or fumed) silica. As a pharmaceutical excipient, colloidal silica is used as an adsorbent, anticaking agent, emulsion stabilizing agent, glidant, suspending agent, tablet and capsule disintegrant and viscosity-increasing agent [2]. Silica is also the main constituent of bioglass, where its relative amount dictates the bioactive properties [3]. In the SiO_2–CaO–Na_2O–P_2O_5 system that constitutes bioglass, bonding to both bone and soft tissue is possible at 52 wt% SiO_2, whereas 52-60% SiO_2 bonds only to bone.

While the conventional colloidal silica is produced via flame hydrolysis of cholrosilanes on industrial scale, more sophisticated methods have been developed to produce silica materials with controlled properties on the nanoscale for research purposes. A colloidal approach for preparing ceramic amorphous metal oxides with high reactivity is the sol-gel process, which not only allows different morphologies (powders, fibres, monoliths, coatings and thin films) to be prepared, but also introduces porosity into the matrix; both properties of which cannot be obtained with conventional ceramics. The porosity of these matrixes paved the way for them to be loaded with active substances, and incorporation of drugs into sol-gel derived silica matrices was introduced as early as 1983 [4] after which sol-gel processed porous silica materials have proven to possess considerable potential as drug delivery carriers. The simplicity and yet, simultaneous versatility of the sol-gel derived materials lies in it being a low-temperature process, where 'green state' ceramics can be prepared at room temperature and ambient pressure. Consequently, the method allows for encapsulation of active and even highly fragile or sensitive molecules, such as biomolecules, into the material already at the synthesis step. This feature thus also allows molecular imaging agents to be incorporated into such materials, and benefit from the stabilizing ceramic matrix in the same manner as incorporated drugs or biomolecules.

Since amorphous silica in itself is optically transparent, the utilization of silica materials usually requires the incorporation of imaging agents into the silica matrix to render the material detectable. This is in contrast to most inorganic materials, that do possess inherent visibility e.g. by some optical or magnetic imaging modality [5]. Conversely, the optical signal of incorporated imaging agents (molecular/nanoparticular) should not suffer considerably by encapsulation into a silica matrix, but instead gain benefit from the shelter of the ceramic matrix (as mentioned above). This approach has been exploited for many years to construct non-porous fluorescent silica nanoparticles incorporated with a range of different molecular fluorescent dyes, utilized for a variety of bio/med/tech-related applications [6]. The most known silica NPs of this type would perhaps be the "C-dots" (Cornell Dots) that entered clinical trials in 2010 as an intravenously administered cancer diagnosis imaging agent. In all of these NP designs, the dye-rich core is protected by a solid silica outer shell.

With the advent of porous silica materials, and especially so the class of ordered mesoporous silicas in the beginning of the 1990's, another strategy for incorporation of active molecules into silica materials emerged. Namely, in these cases, where the synthesis strategy bears origins with zeolite synthesis but instead of using molecular templates for creating the pores, mesoporous materials are synthesized using supramolecular surfactant aggregates as pore templates leading to much larger pore sizes than possible via the zeolite approach. This synthesis approach basically allows for a molecule of any size to be fit inside the pores into the ready material; thus constituting a very versatile carrier for active compounds. In the beginning of the new millennium, these materials were introduced into the biomedical field as drug delivery carriers, and a few years later when mesoporous silica in nanoparticulate form (i.e. mesoporous silica nanoparticles, MSNs) took over this research field, the necessity for labeling the MSNs emerged, as these were studied in cellular systems for intracellular delivery. Nevertheless, since most commercially available fluorophores are designed for bioconjugation with proteins, these could equally well be applied to MSNs bearing surface functional groups – mostly amines, as the fluorophores are also amine-reactive dyes. This has become a standard procedure within the last decade, but applying such materials as imaging agents presents itself with some further complexities that will be discussed in the following chapters.

1.2 SYNTHESIS OF SILICA NANOPARTICLES

The prospects of using silica as a construct in nanoscopic imaging agents is multifold. First, for non-porous silica nanoparticles, molecular dyes can be incorporated into the silica matrix itself, or in the interior forming a dye-rich core that finally is encapsulated into a solid silica shell; or the dyes can be introduced via a layer-by-layer technique where dye-rich layers are sandwiched between layers of solid silica. The outermost silica layer serves to protect the incorporated dyes from the surroundings. Second, for mesoporous silica, the imaging agents can be conjugated to the pore walls via surface functional groups, the molecular agents can be loaded into the pores without chemical bonding or ionic species can be doped into the silica matrix itself. Third, both porous and non-porous silica shells can be coated onto inherently detectable nanoparticles, where the shells can further incorporate imaging agents in accordance with the above-listed approaches to create multimodal imaging agents [5]. In the following, we shall outline in brief the synthesis approaches used for the fabrication of these different types of silica-based imaging probes.

1.2.1 *Non-porous silica*

Non-porous silica nanoparticles are essentially synthesized via two different approaches:

- The so-called Stöber process
- The reverse microemulsion technique

Both of these synthesis methods rely on sol-gel chemistry. On the most fundamental level, the sol-gel process involves the preparation of nanoscale particles (colloids), forming a dispersion i.e. the sol, using inorganic or more commonly, organic alkoxide precursors. The sol reacts further to form another, reversed, dispersion i.e. the gel. If the precursor is a silicon alkoxide, $Si(OR)_4$, molecular polymerization through a series of hydrolysis and condensation reactions occur via the following reactions:

$$\equiv Si - OR + H_2O \underset{\text{(esterification)}}{\overset{\text{hydrolysis}}{\leftrightarrow}} \equiv Si - OH + ROH$$

alcohol condensation (alcoxolation)
$\equiv Si - OR + HO - Si\equiv \leftrightarrow \equiv Si - O - Si\equiv + ROH$
(alcoholysis)

H_2O condensation (oxolation)
$\equiv Si - OH + HO - Si\equiv \leftrightarrow \equiv Si - O - Si\equiv + H_2O$
(hydrolysis)

Commonly ammonia (in basic preparations) or a mineral acid (in acidic syntheses) are employed as catalysts. Iler proposed that polymerization of silica occurs through a mechanism where silicic acid monomers first polymerize into colloidal nanoparticles forming a new population of monomers that in turn increase in size and aggregate into chains and networks, finally forming a gel.[7] Both reactions proceed in parallel but in different extent depending on the conditions employed. The three-dimensional particles serve as nuclei and further growth proceeds by an Ostwald ripening mechanism. In this process, particles grow in size and decrease in number as highly soluble small particles dissolve and reprecipitate on larger, less soluble nuclei. Growth ends when the difference in solubility between the smallest and the largest particles become insignificant (dissolution-reprecipitation). The rate of reactions depends on factors such as temperature, pH and component concentrations.

Employing this chemistry in a controlled fashion, the Stöber method is still one of the most used chemical approaches employed to prepare non-porous silica materials of uniform size, and was discovered in 1968 by Werner Stöber et al. [8], but built on earlier work of by G. Kolbe in 1956 [9]. Kolbe developed the synthesis of monodispersed silica particles based on the hydrolysis and subsequent condensation of silicon alkoxides in ethanol, whereas Stöber et al. systematically worked on the experimental conditions of this reaction and investigated the controlled growth of spherical silica particles, which is now the well-known Stöber process. The use of ammonia as morphological catalyst and the resulting pH was concluded to be responsible for particle monodispersity. Via this synthesis approach, silica nanoparticles with controlled sizes from 50 nm to 2 μm can be prepared. Despite appearing like solid silica particles after synthesis, the macroscopic particle actually consist of granular silica

nanoparticles of a few nanometers in size. Consequently, the Stöber silica particles are in general microporous and this microporosity may even be tuned by slightly modifying the synthesis conditions [10].

Given that the a silicon alkoxide $Si(OR)_4$ used as silica source in sol-gel processing can be partly substituted by organosilanes, $Si(OR)_3$-X, where X is an organic linker terminated with a functional group (or the functional group directly) provides considerable versatility in introducing organic groups into the silica matrix. Since the functional groups also serve as reactive sites for molecular imaging agents such as fluorophores, pre-reaction of organosilanes with dyes serves as the basis for the synthesis of fluorescent silica nanoparticles. There are in essence three strategies for incorporating dye molecules into non-porous silica nanoparticles (**Figure 1**). Type 1 is the physical incorporation of the dye molecules during the synthesis, whereby the dye molecules are encapsulated into the nanoparticles during formation via the sol-gel process by simply adding dye molecules into the synthesis mixture. Literature studies have revealed that entrapped dye molecules via this route exhibit a higher quantum yield and enhanced photostability than corresponding free dye molecules [11]. This procedure is also often referred to as "doping". Type 2 is the above-described, commonly employed strategy involving chemical conjugation of the dye molecules within the silica matrix, which is realized via co-condensation between the main silica source and a dye-conjugated organosilane during the synthesis. Here, the ratio between the silanes need to be carefully adjusted so as not to distort the formation of the nanoparticles, but compared to the Type 1 approach the incorporation yield of the dye into the silica matrix under non-covalent bonding is poor and dependent on the adsorption force between the dye itself and the silica precursor. In type 3, the dye molecules are introduced via post-synthesis procedures. Either the nanoparticle is of co-condensed type, whereby dye molecules can be reacted to the functional group on the particle surface; or the pristine silica surface of the nanoparticle is reacted with pre-reaced organosilane-dye conjugates. The organosilane is typically an aminosilane, most often 3-aminopropyltriethoxysilane (APTES). Although surface conjugation is relatively more straightforward than direct incorporation into the silica matrix, the long-term stability under physiological environments is considered as the limitation during application since all the dye molecules are exposed on the particle surface.

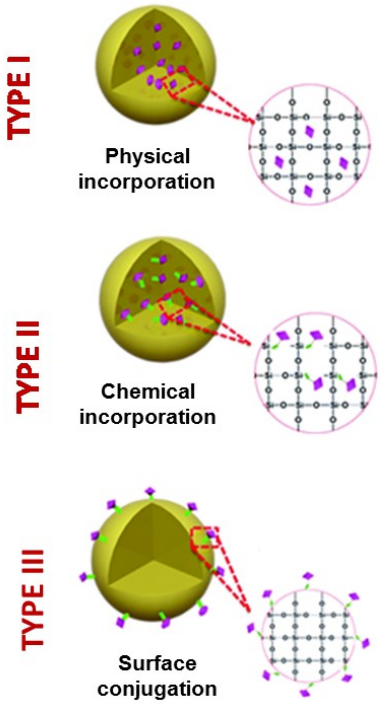

Figure 1. Incorporation of fluorophores into non-porous silica NPs of Stöber type. Type 1: physical incorporation; type 2: chemical incorporation by organosilane chemistry; type 3: Surface conjugation. Adapted from [12].

The reverse microemulsion method is the other general method used for the production of non-porous silica nanoparticles, whereby the resultant silica particles usually yield within a diameter range of tens to a few hundred nanometers. This method is based on the formation of silica nanoparticles in inverse micelles compartmentalized by a suitable surfactant in a nonpolar organic solvent, usually cyclohexane (**Figure 2**). This method was reported in 1999 by Arriagada et al. who synthesized ultrafine silica nanoparticles within an optimized nonionic water-in-oil microemulsion system [13]. The size of the particles can be altered by changing the kinetics of hydrolysis and condensation processes and the ratios among the contents of the microemulsion (i.e. continuous phases, co-solvent amounts and surfactant) but is in general more difficult to control than NPs synthesized via the Stöber synthesis.

The dye incorporation is essentially realized via either doping (addition of dye into the water droplets, in which the silica NPs form) or pre-reaction with an organosilane that is subsequently used in the synthesis [14]. Typical for NPs synthesized via the reverse microemulsion method is that a second silica layer is deposited around the dye-rich core, which prevents the dye molecules from leaching out from the core (in the case of doped dye molecules) and protects the incorporated dyes from the environment (in both cases) from affecting the dye properties, which may vary significantly depending on the surrounding conditions. To this layer may then be added e.g. APTES-organosilanes to facilitate bioconjugation, i.e. coupling of biomolecules to the particle surface. Furthermore, a second set of fluorophores could also be incorporated into this second silica layer and conjugated to the surface, thus enhancing the fluorescence; denoted fluorescent double-layered silica nanoparticles (FL-DLSN) (Figure 2) [15]. This outer silica layer is typically grown using the Stöber approach, and is thus susceptible to hydrolytic stability issues if the main aim is to protect the dyes in the core from leaching [16]. This is due to the mode of silica growth resulting from the Stöber synthesis discussed above, i.e. very small silica nanoparticles aggregating together to form larger structures. As mentioned above, the resultant materials may appear as macroscopically solid but actually are microporous. This microporosity renders these materials susceptible to hydrolytic degradation in aqueous environments. More recent methods have thus been developed to create more dense silica shells, such as for instance biosilicification related methods in water (in which amino acid residues are used to control the reaction) have shown to generate silica shells that are resistant against dissolution around Stöber silica cores in which the dyes are incorporated [16].

In addition to the reverse microemulsion method, also the oil-in-water microemulsion system (instead of water-in-oil) can be used to prepare silica NPs that uses "normal" micelles instead of reversed ones (Figure 2). In this method, the non-polar core is used for hydrolysis and condensation of an organosilane as silica precursor, e.g. vinyltriethoxysilane (VTES) [17]. Here, the surfactant properties dictates the size of the final silica NPs. Owing to the 'nanoreactor' conditions in both microemulsion based methods (where the micelles serve as the nanoreactors for the formation of the silica NPs) the reverse microemulsion method (polar core) is especially suitable for encapsulating hydrophilic dyes or nanoparticles,

while the opposite is true for the approach using regular micelles (non-polar core).

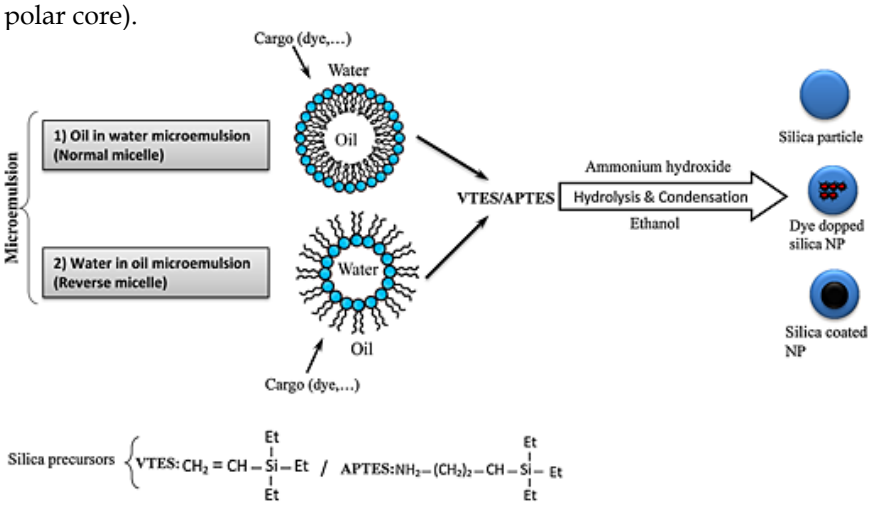

Figure 2. Overview of microemulsion methods to synthesize silica NPs. 1) Oil-in-water microemulsion method, in which the hydrolysis and condensation of an organosilanes occurs within normal micelles and then APTES is used for presenting amine groups on the surface of the nanoparticles. (2) Water-in-oil microemulsion (reverse micelle) method. Various cargos such as organic fluorescent dyes or other nanoparticles can be doped or encapsulated within silica particles through both of these methods. From [17].

Many names can be discerned that have been devoted to fluorescent silica NPs. Besides the already mentioned C-dots or Cornell Dots [18,19], developed at Cornell University; likewise, the so-called FloDots derived their name from being developed at the University of Florida [20]. While the C-dots are prepared via a modified Stöber process (also involving deposition of a second, solid silica layer around the dye-rich core NP) the FloDots can be prepared both via the Stöber and reverse microemulsion methods. The oil-in-water microemulsion method has been mostly used to synthesize so-called ORMOSIL (organically modified silica) nanoparticles [21,22].

1.2.2 *Mesoporous silica nanoparticles (MSNs)*

The synthesis of mesoporous silica materials dates back to the beginning of the 1990's, when the groups of Kato et al. and Mobil Oil researchers

independently from each other reported on the synthesis of a silicate material with hexagonally ordered pore structure, but via different synthesis approaches [23,24]. The Mobil Oil approach included synthesis of ordered mesoporous materials by using isotropic supramolecular surfactant aggregates as templates, around which inorganic material deposits via the sol-gel process forming a mesoscopically ordered hybrid organic-inorganic composite material. The organic template was subsequently removed via calcination, leaving the porous silicate network with ordered pore structure. This provided a novel route to make highly ordered nanocomposites that are difficult to prepare by traditional routes, and allows a precise control and design of architecture of the ceramic materials on the nanometer-scale. The original syntheses were based on self-assembly principles in surfactant solutions by the crystallization of aluminosilicate or silicate gels in a concentrated solution of alkyltrimethylammonium ions [25]. These materials are characterized by their well-ordered structure, tunable pore size from 1.5 to 10 nm, and simple preparation methods. The main components in the synthesis are essentially the same as for Stöber silica NPs, i.e. a source of silica, a solvent, and a catalyst, typically an acid or a base; with the addition of structure-directing surfactants as pore templates. In principle, the self-assembled liquid crystals from the surfactant act as a template to support the growth of the ceramic materials (**Figure 3**) [26]. The amount of reported syntheses and accompanied synthesis mechanisms in the literature are extensive, but in 2009 a review was published that compiled a large number of verified syntheses for mesoporous materials [27].

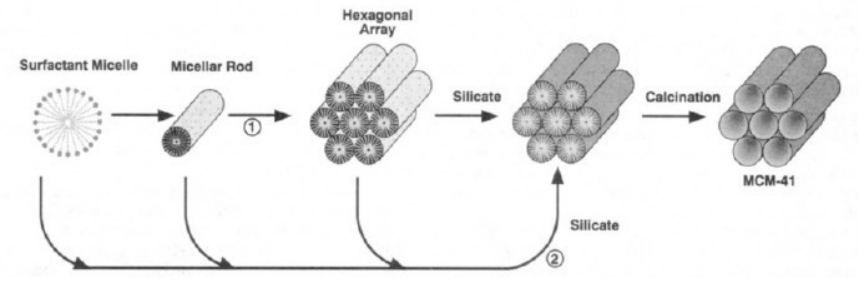

Figure 3. Possible mechanistic pathways for the formation of hexagonally ordered MCM-41 as originally proposed by the Mobil Oil Research group: (1) Liquid crystal initiated and (2) silicate anion initiated. From [25].

In the 2000's, when mesoporous silica entered the biomedical research field, the particle size also became important to control on the nanoscale. Essentially the particle size can be controlled by employing the principles from the Stöber synthesis; but given the dilute conditions used the yield is typically quite low. In order to improve the reaction yield of nanoparticles, the addition of growth quenchers such as other surfactants, triethanolamine or ethylene glycol was introduced instead [28]. Considering the reaction conditions, pH, reaction temperature, type of silica precursor and even stirring rate can have a profound impact on particle size [29]. Numerous syntheses on MSNs of different sizes, typically within the range of 30-300 nm have been reported, but it seems inconclusive that a general rule for size control over the full nanoscale would exist to date. Regardless of syntheses yielding monodisperse MSNs in the synthesis solution, it is usually the post-synthesis handing and treatment that has proven to be crucial for maintaining the dispersability of the MSNs. To avoid self-aggregation during synthesis, the template removal is usually carried out via solvent extraction methods for MSNs. Most often, the next step involves surface functionalization, to prevent aggregation during further processing (labeling/ drug loading/ biofunctionalization/ introduction of stimuli-responsive functions/etc.) or drying steps, and in later stages to ensure proper interactions at the nano-bio interface [30]. Surface functionalization is generally carried out for MSNs via two different approaches: co-condensation or post-synthesis grafting of organosilanes (i.e. the same as for the non-porous silica NPs). In the co-condensation approach, the functional organosilanes are added already in the synthesis step together with the main silica source (most often TEOS) and thus the functional groups are homogeneously distributed throughout the silica matrix (**Figure 4A**). In the post-synthesis grafting approach, the organosilane is reacted with surface silanols of the already formed MSNs (**Figure 4B**). This approach usually leads to a higher amount of accessible surface groups than the co-condensation approach, but typically the groups are congregated close to the pore entrances.

Similarly as for non-porous silica NPs, the incorporation of fluorescent dyes is most often realized by pre-reacting with the organosilane (most often APTES) [31] that is subsequently used for either co-condensation or post-synthesis grafting reactions. Depending on the dye, care must be taken that it is not subject to any inactivating conditions during these

reactions e.g. high temperature, incompatible solvents and so on [32]. To avoid such incompatibilities, the dye can also be conjugated to an already surface functionalized MSN. Most commercial dyes are amine-reactive, so APTES is suitable also in this case. If a higher dye loading is desired, the dye can also be conjugated at later stages if amine-rich polymers (such as polyethylene imine, PEI) is used for further surface functionalization [33–35]. Dye loading degrees achieved via covalent conjugation are typically in the range of a couple of weight per cent at maximum. In the case of fluorescent dyes, however, the maximal amount loaded does not at all necessarily correlate with optimal fluorescence intensity signal; which is an issue we will return to in chapter 1.3 below.

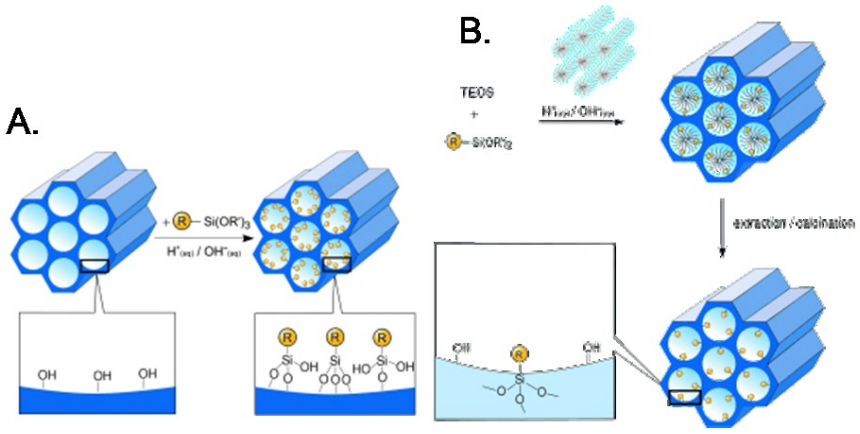

Figure 4. Surface functionalization with functional organosilanes via the co-condensation process versus the post-synthesis grafting approach [31]. "R" is the functional group.

1.2.3 *Core@shell particles*

1.2.3.1 *Non-porous shells*

Among all core@shell constructs, inorganic/inorganic nanoparticles have been claimed to be the most important class of core/shell nanoparticles and amongst these, silica is the most common construct/coating [36]. The use of silica as a coating material for other inorganic nanoparticles is thus widely applied, and the rationale is multi-fold. Coating with non-porous

silica is commonly applied to enhance the dispersability of nanoparticles, especially in aqueous solvent, due to the inherent hydrophobicity of most other inorganic nanoparticles. Deposition of a silica coating further provides enhanced colloidal/chemical/photo/thermal stability to the core material, controlled porosity and surface chemistry, facile processing, and optical transparency. A typical example is coating of iron oxides with silica, which introduces hydrophilicity and biocompatibility and simultaneously allows for easy further functionalization, while protecting the core material against pH changes in the environment, which otherwise can lead to e.g. oxidation or even full dissolution of the core material. Protection from an aqueous environment is also one reason for frequently coating UCNPs (upconverting nanophosphors) with silica, as contact with water is prone to quench the optical signal for many UCNPs [37,38]. In the case of quantum dots (QD) silica coatings are often applied to enhance the biocompatibility and aqueous dispersability of the QDs. Silica coatings have also been used e.g. in photoacoustic imaging for increasing the photothermal stability of the Au [39] or superparamagnetic iron oxide (SPION) core materials [40], or in magnetic resonance imaging (MRI) to modulate the relaxivity of maghemite (γ-Fe_2O_3) nanoparticles [41].

Coating of inorganic nanoparticles with non-porous silica shells can be conducted via both the Stöber method as well as the reverse microemulsion method. Prior to coating via the Stöber method, an organosilane is usually first used to 'activate' the surface of the NP, after which the hydrolysis and condensation reactions of added TEOS can proceed from the NP surface. By adjusting the amount of silica precursor, it has been reported that this approach can be used to control the resulting shell thickness from a couple of nm to several hundred nm. Also the reverse microemulsion can reportedly be utilized to control the thickness of the silica coating on inorganic NPs within a few tens of nanometers. If the core NPs are hydrophilic, the NPs can be solubilized in the water-filled micelles directly; otherwise a silane coupling agent (organosilane) like in the case of coating via the Stöber method, or polymer stabilizer are needed to render the NP water dispersible prior to coating. Gold (Au), silver (Ag), nanodiamonds (ND) [42], different types of iron oxides and QDs of type CdSe, CdSe/ZnS and CdSe/ZnSe/ZnS have been coated using these methods [17].

1.2.3.2 *Mesoporous shells*

The prospect of coating inorganic NPs with mesoporous shells was manifested from the attempt to create imaging probes with in-built drug delivery capacity (at the time referred to as "theranostic probes") and was reported for the first time in 2006 for hydrophobic iron oxide and quantum dot nanocrystals [43]. In these syntheses, the structure-directing agent (SDA), most often CTAB, serves a double purpose. In the first step, it functions as a phase-transfer agent to transfer the hydrophobic cores from non-polar organic phase to aqueous phase. In the following step, the SDA should also serve its general purpose as a pore template. The formation of the mesoporous shell subsequently proceeds as a liquid-phase seeded growth approach [44], where the pre-existing cores serve as nucleation seeds for the propagation of the mesoporous shell. The final size and uniformity of the resulting core-shell particles are greatly affected by the self-assembly of CTAB/silica mesostructured assemblies onto the CTAB-stabilized cores [45]. The self-assembly process follows the same principles as the synthesis of pristine MSNs, with the distinct difference that no seeded growth is taking place in the synthesis of pure MSNs [46]. Similarly as for prisitine MSNs, pore swelling can be attempted also for porous shells; albeit the synthesis conditions need to be more tightly controlled in the case of shell synthesis and the nature of the pore swelling agent determines the prevailing mechanism (see **Figure 5**). For hydrophilic core materials, no phase transfer needs to take place but the cores are dispersed directly into the synthesis medium. Here, it is crucial that CTAB is used in excess to form a double layer around the core material, in order for it not to precipitate the core from the aqueous phase. Further, successful formation of a porous shell instead of all-silica MSNs is highly dependent on the ratio of the used solvents. For smaller cores, a mesoporous silica coating is often directly deposited while for larger cores a middle layer of non-porous silica is often deposited first to assure proper interactions for further mesoporous silica deposition. For iron oxide beads, the non-porous silica coating may also needed for protection of the core material from further mesoporous silica coating, which generally takes place under either acidic or basic conditions whereby acidic conditions could dissolve the core material. This approach can also, conversely, be exploited for the synthesis of hollow mesoporous silica particles (H-MSNs), where the hollow interior space is templated by nanoscaled cores of a material that can be easily leached out after the synthesis of a porous shell; so-called "hard templating". When one or

several core materials are incorporated into the hollow void of H-MSNs they are usually referred to as rattle-like structures. Such hollow or rattle structures have been constructed out of e.g. UCNPs to provide for luminescence imaging [38] or manganese oxide (MnO) for magnetic resonance imaging (MRI) [47]. Core@shell nanostructures based on hydrophilic core nanoparticles coated with mesoporous shells have to date been synthesized from core materials including e.g. metals such as platinum, gold, and silver or other inorganic NPs such as quantum dots, nanodiamonds (NDs) and upconverting nanophosphors (UCNPs) that are interesting for optical imaging applications. For the construction of Au@MSN NPs, even a one-pot synthesis have been developed [48]. It may also be interesting to note that, if the nanomaterial to be incorporated is too small for core-shell composite formation, other types of nanocomposites can be constructed besides core@shell structures. For instance, in the case of luminescent Carbon Dots (CDs) with typical sizes well below 10 nm, these can instead be incorporated either into the pores of MSNs via *in situ* synthesis using the mesopores as nanoreactors [49], or outside the pores as gate-keepers [50].

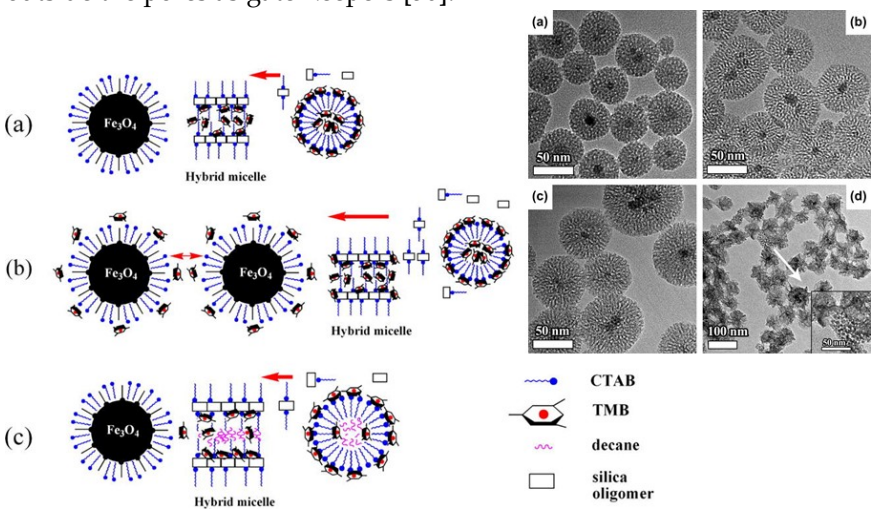

Figure 5. Schematic illustration of the proposed mechanism for the growth process of silica/CTAB mesophases on magnetic cores in the presence of different pore swelling agents: (a) TMB only, at low TMB/CTAB molar ratio; (b) TMB only, at high TMB/CTAB molar ratio; (c) Joint incorporation of TMB and decane, at high pore swelling agent/CTAB molar ratio. The left-pointing red arrow represents the growth process of mesostructure on the nanocrystal core, and the bidirectional red arrow represents the interparticle interaction. From [46].

1.3 SILICA NANOPARTICLES FOR IMAGING

Given that silica in itself does not possess any imaging activity, the rationale for using all-silica nanoparticles as imaging probes relates to their use as carriers for molecular imaging agents or other, smaller nanoparticles. There are several advantages that can be achieved by incorporating imaging agents into nanoscaled carrier particles:

- Sensitive agents can be provided *long-term physical, chemical and photostability*
- Protection of molecular agents against potential *enzymatic or hydrolytic degradation* in the body
- Particle carrier can be designed to *provide access to sites unreachable by the molecule itself* (crossing of physiological barriers)
- Achieve *cellular targeting and uptake* → enhanced accumulation of imaging agent at the target site → lowering of administered dose
- Particles can be designed to be *long-circulating* (stealth properties)

1.3.1 *Silica nanoparticles as carriers for optical imaging agents*

Many advantages of silica-based nanoparticulate fluorescent probes have been identified early on, including: [20]

- *High emission intensity*: a large number of fluorescent molecules can be encapsulated into a single NP, giving rise to strong emission signals under the right conditions
- *Excellent photostability*: photobleaching is one of the major problems for traditional fluorescent dyes, but owing to the protection and shielding effect of the silica matrix the incorporated dye molecules are well protected from the surroundings including environmental oxygen, leading to constant fluorescence enabling accurate measurements
- *Water dispersability and efficient conjugation*: silica is a hydrophilic material that is biocompatible and readily dispersible in aqueous media, both required for biomedical applications; and the silica surface is flexibly surface functionalized via different methods enabling facile conjugation of biomolecules or other active moieties to the silica particle surface.

However, the properties of the incorporated fluorescent dyes are not additive, but the resulting fluorescent properties largely depend on the architecture of the silica NP construct as well as the vicinity to neighboring dyes and polarity of the most immediate surroundings, amongst other things. In NP structures encompassing a dye-rich core, fluorescence quenching is prone to occur either via intraparticle energy transfer or some other nonradiative pathway (e.g. molecule-molecule interaction, electron transfer, isomerization) within the solid matrix [19]. Webb and co-workers aimed to control the photophysical properties of C-dots through nanoparticle architecture, and studied three different structures to investigate how the particle structure could either ameliorate quenching or even lead to fluorescence enhancement (**Figure 6**).

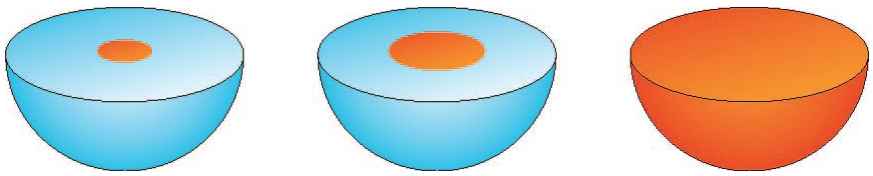

Figure 6. Schematic representation of three different silica nanoparticle architectures, detnoted from left to right as 1) a compact core–shell particle containing dye surrounded by a silica shell, 2) a slightly expanded core/shell particle, and 3) homogeneous particle with dye molecules sparsely embedded within the matrix. Blue designates silica without dye molecules; orange designates a composite silica dye matrix. From [19].

They observed a greater than 3-fold increase in the quantum efficiency of fluorescence of tetramethylrhodamine by optimizing the NP structure, and each architecture gave a 2-fold enhanced radiative rate for the constituent dye. The reduction in nonradiative rate varied by a factor of 3 between the architectures, with the lowest nonradiative rate observed for the homogeneous particle. These changes in nonradiative rates correlate with the restricted rotational mobility of the within the particle covalently bound dyes: the more restricted the mobility, the smaller the nonradiative rate. No direct evidence for intraparticle energy transfer between dye molecules was observed. As a conclusion, the authors suggested that dyes with large absorption cross-section and low quantum efficiency might benefit from being encapsulated within NPs. This property is dependent on the spectral characteristics of added dye *e.g.* the overlap of excitation and emission spectra *i.e.* Stokes' shift.

In the case of fluorescent metal–antenna-chelates that employ Förster resonance energy transfer (FRET) from the chelate to e.g. lanthanide ion, doping, silica in the reverse microemulsion strategy helps to serve three goals: a simple chelate structure could suffice as other ligands could not freely compete from the coordination sites of the metal ion, dynamic quenching of the long-lived fluorescence could be excluded and very hydrophobic constructs could be used as the surrounding silica shell would counteract any problems in solubility [51]. Lanthanide chelate - labels have extremely long Stokes' shift due to the FRET between chelate-antenna and emitting metal-ion. This property allows high local concentrations of the label to be packed inside the NPs, because self-quenching observed with many organic fluorophores is nearly eliminated by the low-energy (higher wavelength) emission [52].

For mesoporous silica the situation may become even more complicated, due to the additional confinement effects created by the constraints of the nanosized mesopores, including overlapping surface potentials, differing conditions inside the pores compared to the outside etc. [53,54]. Also in the case of mesoporous silica, the dyes can either be loaded into the pores without any chemical bond or conjugated to the pore surfaces by *in situ* (co-condensation) or post-synthesis functionalization methods. Before doing so, the dye properties should be taken into account to avoid inactivation of the dye during incorporation. Such contributing factors may include solvent incompatibilities, inappropriate pH or temperature exposure, creating of high local abundance of acidic or basic groups that may affect the fluorescence properties of the incorporated dye and so on (**Figure 7**).

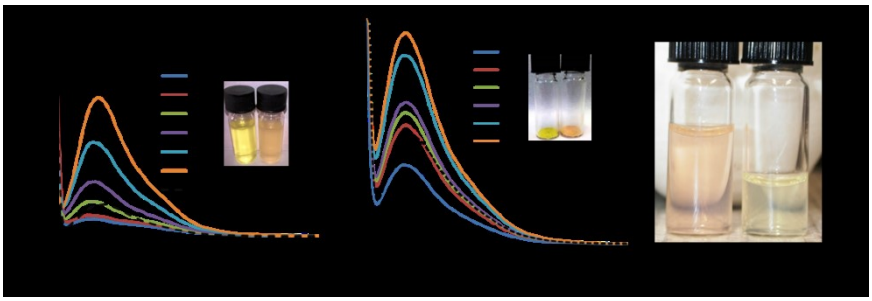

Figure 7. Dependence of FITC-conjugated MSN (F-MSN) fluorescence intensity as a function of pH. a) F-MSN fluorescence intensity variability with solvent pH. Coating with 25k PEI (10 wt%) via electrostatic adsorption results in the same emission spectra regardless of solvent pH. Inset: F-MSNs (left) vs PEI-F-MSNs (right) in HEPES buffer. b) Same as previous repeated for a second set of MSNs with surface-grafted PEI, resulting in an enhanced local pH drop due to PEI residing also inside the mesopores. Inset: dry FITC-conjugated MSNs vs PEI-MSNs. Non-porous (Stöber) control particle. On the left PEI-SiO_2 (+39 mV surface charge, $\lambda_{max,Abs}$=501.5 nm, $I_{max,fluo}$=174) and on the right the same particle but further succinylated (-42 mV surface charge, $\lambda_{max,Abs}$= 488 nm, $I_{max,fluo}$=547) as measured in HEPES buffer at pH 7.2. From [35].

In this case, the most common fluorophore in MSN context, fluorescein isothiocyanate (FITC), was used. Fluorescein is well-known to be pH-sensitive, and thus, not only the surrounding pH will have a marked effect on the signal readout but also the local surroundings of the dye in the mesopores will have an impact. In Fig. 7, while the MSNs are not surface functionalized (except for the APTES used to conjugate FITC to the silica matrix) the fluorescence behavior follows what could be expected from the surrounding pH, while after functionalization with the polybase PEI, the local pH effect of PEI becomes dominant. Further, a pronounced absorbance peak shift is observed as a color change in the figure, indicating a change in polarity in the immediate surroundings of the dye.

Further, the dye concentration inside the pores as well as the particle concentration will have a profound impact on the fluorescence intensity. Upon investigation of the dependence of dye loading degree of fluorophores in MSNs on the fluorescence intensity, the loading degree of both hydrophilic fluorescein (incorporated by conjugation) [55] and hydrophobic carbocyanine dyes (incorporated by adsorption) [32] was found to be around 1 wt-%. Beyond this dye loading degree, rapid self-quenching occurs most likely due to a FRET (fluorescence, or Förster, resonance energy transfer) effect (see **Figure 8a**).

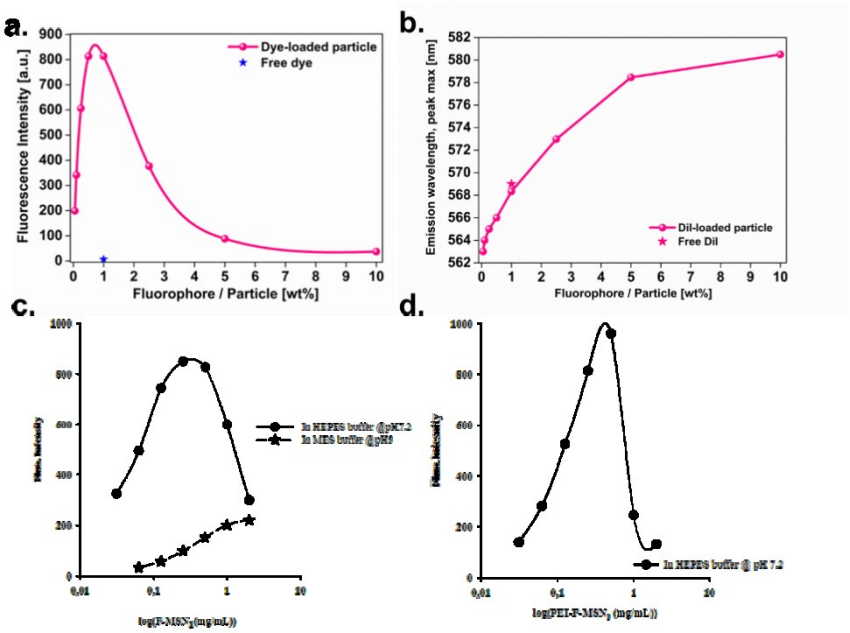

Figure 8. Dye loading degree and MSN concentration dependence on fluorescence emission properties. a) Fluorescence intensity as a function of hydrophobic DiI fluorophore loading into MSNs; b) Shift in maximum emission wavelength as a function of hydrophobic fluorophore loading into MSNs. Fluorescence intensity as a function of MSN concentration for c) F-MSNs; d) PEI_{ads}-F-MSNs. From [32].

A maximum emission wavelength peak shift of up to almost 20 nm can also be observed when going from loading degrees of 0,1 wt% to 10 wt% for hydrophobic fluorophore loading into MSNs (Fig. 8b). Interestingly, the same intensity dependence is observed as a function of MSN

concentration (Fig. 8c & d) and again, for non-surface functionalized MSNs the intensity variation is further dependent on the surrounding pH (Fig. 8c). These observations suggest that great care should be taken when attempting to use fluorescence intensity as a quantitative measure, especially for pH-sensitive fluorophores. Depending on intracellular location, the pH tend to vary between 5-7 and further, NPs tend to accumulate in intracellular compartments, which, according to above, could lead to quenching effects.

An even greater concern upon using fluorophore labeling is the imminent risk of dye leaching; especially for mesoporous NPs with an open pore structure with efficient water access. As the detection of MSNs is completely relying on the detection of attached labels, is must be assured the label is indeed still associated with the NP carrier. As mentioned above, significant dye leaching has been observed even in the case when the dyes are incorporated within the core of a non-porous particle, surrounded by a siliceous shell (**Figure 9**) [16]. This is due to the hydrolysis of the silica shell, the kinetics of which is promoted by the microporosity of Stöber derived silica coatings.

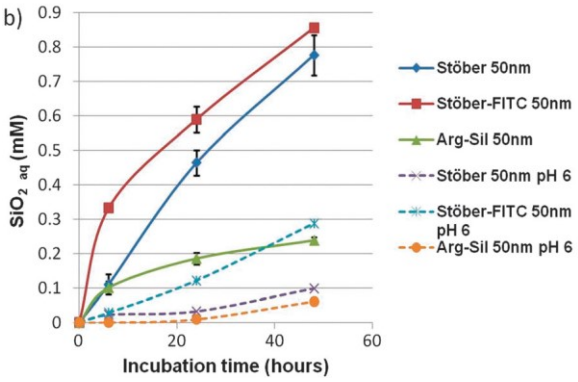

Figure 9. Dissolution of SiO_2 NPs monitored by the molybdenum blue assay incubated in buffer (100 mg/ml, HEPES pH 7.4, NaCl 148 mM, $CaCl_2$ 1 mM at 37ºC and HEPES pH 6, NaCl 148 mM, $CaCl_2$ 1 mM at 37ºC). From [16].

MSNs with typical wall thicknesses of 1 nm are consequently even more sensitive to hydrolysis, which inevitably in parallel leads to leaching of attached dye molecules even if the chemical bond itself would be stable against hydrolysis. In **Figure 10**, FITC- and TRITC- (tetrarhodamine isothiocyanate) conjugated MSNs with and without PEI-coating were investigated for their dye leaching kinetics. Very different leaching behavior was observed that could be ascribed to the different characteristics of the dye molecules and their interactions with the silica surface (modified or not). Due to the static conditions used, re-adsorption of dye could also be observed under favorable conditions. Overall, a combined dissolution-reprecipitation (of silica) and adsorption-desorption (of fluorescent labels) equilibria is what is most likely being observed [35]. Under application (*in vivo*) conditions, re-precipitation and re-adsorption effects are more likely to be absent due to much higher liquid volumes available combined with continuous solvent exchange. Under intracellular conditions, however, the situation may be very different.

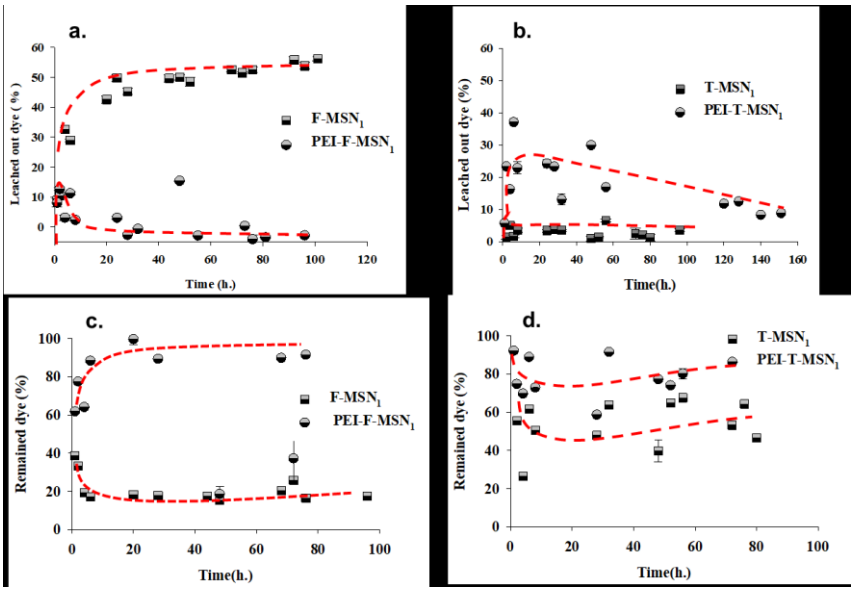

Figure 10. Relative fluorophore leaching percentage based on measurement from the supernatant for F-MSNs (a) and T-MSNs (b). Remaining fluorophore content in the leached MSNs, obtained by dissolution of the remaining MSN cake after separation from the leaching solution for F-MSNs (c) and T-MSNs (d) From [35].

It stands clear from the above that the application conditions should not only be kept in mind when designing appropriate imaging probes. A relatively unexplored area is using the MSNs as carriers for loaded fluorophores, with the intent of delivering the dye inside cells and intracellularly release the dye to stain the cell. As hydrophobic drug molecules are very suitable for this purpose [29], one would expect similar advantages to be gained for hydrophobic dye molecules. On this note, we incorporated a range of different dye molecules into differently surface modified MSNs to yield an imaging probe for cellular labeling (**Figure 11**).

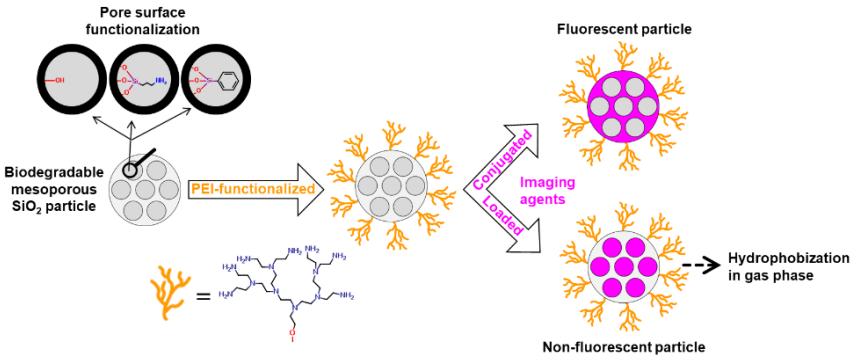

Figure 11. Schematic representation of the particle designs studied in ref. [32].

The rationale behind this study was to find the most appropriate design in terms of surface chemistry (hydrophilic vs hydrophobic), mode of dye incorporation (conjugation vs loading) and dye characteristics (hydrophilic vs hydrophobic) for the most efficient cellular labeling and long-term cellular tracking *in vitro* and *in vivo*. The results revealed that the most long-term imaging probe design out of the almost 40 combinations studied was an MSN loaded with a hydrophobic dye that could release the dye cargo inside the cells in a sustained manner. The intracellular release ability was further confirmed by FRAP (fluorescence recovery after photobleaching) measurements [56]. The labeling efficiency was significantly improved as compared to that of quantum dots of similar emission wavelength, highlighting the potential to utilize the carrier capability of MSNs as a self-generating cellular label instead of inherently detectable NPs (see also section 1.4.2).

1.3.2 *Silica nanoparticles as carriers for MRI, PET, SPECT labels*

Introduction of metal atoms/ions into silica nanoparticles can generally follow three routes: 1) direct substitution, 2) doping and 3) chelation. In the third case, radiolabeling and attachment of paramagnetic complexes to MSNs essentially follow the same procedure; which in the initial stages is not very different to dye incorporation. Both radionuclides (for PET and SPECT imaging) and paramagnetic ions (for MR-imaging) are usually complexed into organic chelates, which can be attached as labels to NP systems. For radiolabeling, the subsequent complexation of radionuclides requires specialized facilities and follows established radiochemical methods, and will thus not be discussed in detail here. We will concentrate on the incorporation of the chelates to silica NPs, for which the complexation of paramagnetic ions can take place either before or after immobilization on or into a NP matrix. Since silica is an inorganic material, direct doping of ions into the silica matrix can also be used as an approach to incorporate different ions [57]. This approach has been studied to some extent for the incorporation of paramagnetic ions such as Gd^{3+} or Mn^{2+} for MRI activity [58], both of which mainly provide *T*1-weighted or positive (white) contrast MR-imaging. Especially for metallic silicon (Si) based materials, radiolabeling via direct incorporation of e.g. fluorine-18 ions [^{18}F] to the surface of the material can also be utilized; where the mechanism of incorporation depends on the material characteristics (**Figure 12**) [59]. Especially porous silicon (PSi) materials have been utilized successfully for these purposes [5,60].

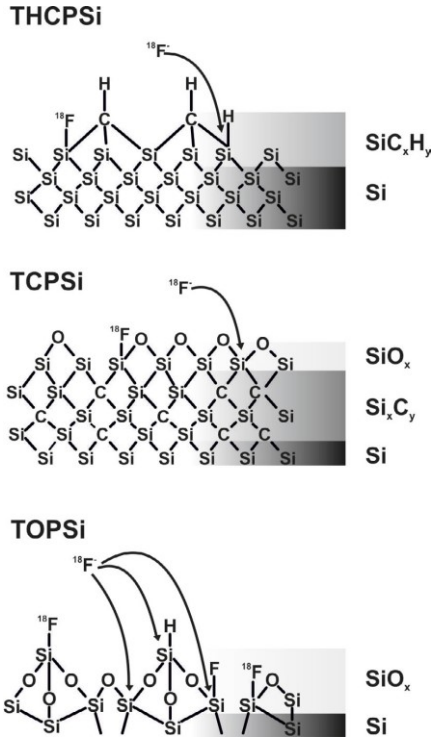

Figure 12. Plausible mechanisms for [^{18}F] incorporation to PSi surfaces [60].

In this case, for thermally hydrocarbonized porous silicon (THCPSi) the radiolabeling reaction has been suggested to proceed via a direct substitution of $^{18}F^-$ to a silyl hydrogen; while for thermally carbonized porous silicon (TCPSi) the incorporation of $^{18}F^-$ is more likely to occur by a nucleophilic attack to the Si–O–Si bridges on the thin silica layer on the Si_x–C_y surface. In addition to the attack to both a silyl hydrogen or to a Si–O–Si bridge, the isotopic exchange of ^{18}F for the residual silyl hydrogen is possible in thermally oxidized porous silicon (TOPSi) with a silica surface. Nevertheless, it is feasible that in all the materials, a Si–^{18}F bond is created [59].

The more conventional method, i.e. conjugation of organic chelating groups such as tetraazacyclododecane-1,4,7,10-tetraacetic acid (DOTA), 1,4,7-triazacyclononane-triacetic acid (NOTA) or diethylenetriamine-pentaacetic acid (DTPA), to NP systems follows essentially the same rationale as dye molecules. The chelates can be entrapped into the NP matrix during synhesis via co-condensation or conjugated to the surface post-synthesis. These chelates correspond to the Gd-based contrast agents that are in use in the clinic under trade names such as Dotarem® (Gd-DOTA) and Magnevist® (Gd-DTPA). The same chelating agents are commercially available with a reactive linker group, again, analogous to most commercially available fluorescent dyes. For the most part, the metal centre (Gd^{3+} ion) is complexed after incorporation to the MSNs, whereas it should be noted that the accessibility of the chelate will be largely dependent on the mode of incorporation [61]. In other cases, the Gd^{3+} ion can be complexed before conjugation to the NP, as the complexation is quite strong. In some cases, the complexation is even carried out prior to being added into the synthesis mixture. In this case, the chelates have been pre-reacted with the aminosilane APTES, whereafter the Gd^{3+} complexation takes place before the silyl-derived Gd^{3+} complexes are used in a co-condensation reaction in the synthesis of MSNs (**Figure 13**). In this specific study, MSNs were synthesized using 10 wt % Gd-1 and 10-40 wt % Gd-2 complexes to investigate the loading efficiency of Gd(III) chelates using this approach. The co-condensastion procedure affords MSNs with much higher loadings of Gd(III) chelates into MSNs, but the r_1 relaxivities still appear to be smaller on a per Gd basis, presumably owing to the reduced accessibility of the Gd(III) chelates to the water molecules [62].

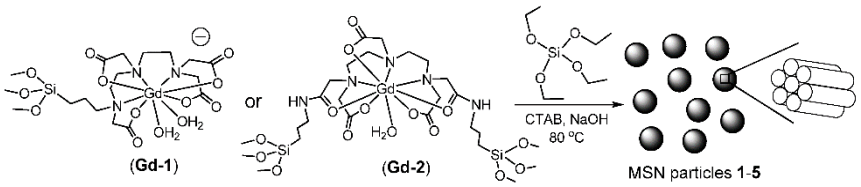

Figure 13. Formation of 1) 3-aminopropyl(trimethoxysilyl)-diethylenetriamine tetraacetic acid (Si-DTTA) and bis(3-aminopropyl triethoxysilyl)-diethylenetriamine pentaacetic acid (Si_2-DTPA) followed by 2) Gd^{3+} complexation to yield derivatives Gd-1 and Gd-2, and 3) co-condensation of these in the synthesis of MSNs.

Consequently, the accessibility of the chelates can be a challenge both in terms of 1) complexation of Gd^{3+} ions, if the chelating groups are conjugated prior to complexation or 2) water accessibility upon MR-imaging, whereas interaction between the magnetic centers and water is essential for the MRI activity (i.e. contrast enhancement). Davis et al. compared the co-condensation approach to post-grafting of Gd-DOTA complexes, and found significant differences in relaxometric properties depending on the location of the Gd-DOTA complex [63]. This provided them with a means to control the relaxivity by location-tuning of the complex by "slow-delay" vs. "long-delay" co-condensation as compared to post-grafting. Deliberately restricting the conjugation of Gd(III) chelates to the outer surface of MSNs thus should maximize the relaxivity of the attached complexes [61], since they will all be rendered active in terms of MR-imaging (water accessibility). The advantage of using a porous matrix in this case may of course be questionable, since a non-porous NP would serve the same purpose. Notably, while the formed bonds between the incorporated chelates and MSN matrix has been deemed to be stable [64], it is worth keeping in mind the hydrolytic stability of material itself (c.f. dye leaching) when considering the stability of the system *in vivo*.

When other rare-earth transition metals, with photoluminescent energy transitions, are complexed into such chelates, the same system can be utilized for optical imaging if the metal ion is e.g. Eu^{3+}, Dy^{3+}, Nb^{3+} or Tb^{3+} [65]. Contrary to the case of Gd-complexes and MRI, these complexes need to be protected from water, as water exposure will lead to luminescence

quenching or suboptimal coordination of the antenna chelates [66]. Here, the metal complexes can preferably be incorporated inside the mesopores, after which the MSN may be coated with a water-impermeable (polymeric) coating to maximize the luminescence under aqueous conditions. The same but opposite strategy is frequently applied in the case of non-porous silica coating of chelate carrying NPs, whereby e.g. Eu-chelates are entrapped into a polymeric NP matrix that is subsequently coated with silica.

Given the size of the chelates as well as the restriction from water if the bulky chelates are located inside mesopores, pore-expanded MSNs are perhaps to prefer in order to render the portion of Gd-complexes incorporated inside mesopores active as well. Another aspect to consider is the theranostic potential of these carriers (see section 1.5.2) whereby the mesopore space may be visioned to be saved for drug loading. In this case, doping of metal ions into the silica matrix can be attempted instead, as these will be incorporated into the matrix itself and not occupy pore space. Guillet-Nicolas et al. [67] prepared MSNs with 3D and 2D pore network connectivity by introducing the Gd^{3+} ions into MSNs by the incipient wetness technique, thus creating $GdSi_xO_y$ MSN hybrid systems and compared their relaxiometric properties. The 3D pore connectivity provided a significant increase in r_1 relaxivity compared to the 2D pore geometry (and 4.6 times higher relaxivity than free Gd-DTPA) most likely due to the more open structure and hence, increased water accessibility and diffusivity within the 3D pore structure. These results were corroborated by Şen Karaman et al. [68], who studied a range of different incorporation methods and MSN structures to find the optimal preparation route for maximizing the r_1 relaxivity (**Figure 14**). Parameters under study included the structure of the MSN matrix, post-synthesis treatment protocols, as well as the source and incorporation routes of paramagnetic Gd^{3+} centers. Also here, the best results in terms of relaxivity were obtained with a hollow MSN structure with expanded pore size, most likely due to the enhanced water accessibility compared to regular MSN structures. Such modulation of the MSN structures to maximize relaxivity thus allows for minimization of the Gd dose, which is of utmost importance from a clinical perspective since Gd is quite a toxic element. The enhanced relaxivity frequently observed for NP-immobilized MRI contrast agents is not only owing to water accessibility (which may be

more relevant for porous systems) but also the resulting slow global tumbling rates [69]. Additionally, all the benefits of having imaging agents incorporated in a NP matrix is highly valid also in the case of MR-imaging; besides the lowered dose also e.g. prolonged imaging time-frame, crossing of biological barriers, cellular uptake and retention, cellular and tissue targeting potential with long-circulating properties, leading to enhanced accumulation at the target site and so forth.

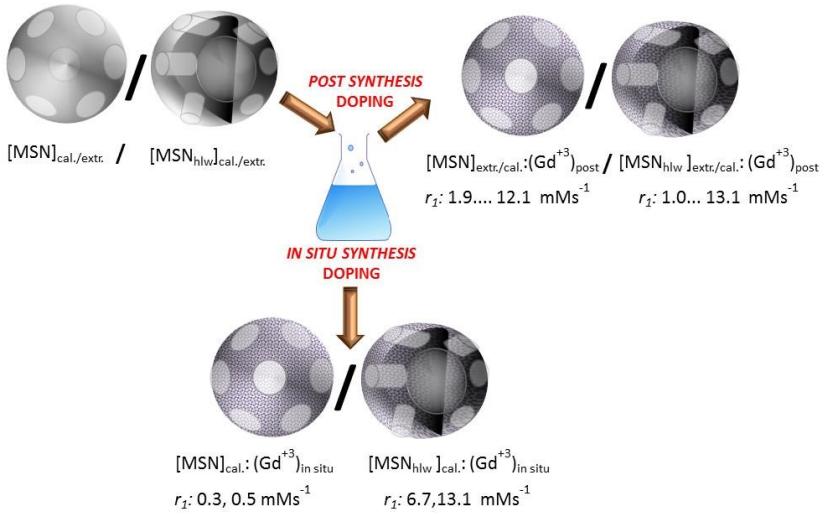

Figure 14. Incorporation of Gd-ions into MSN matrices by varying *in situ* synthesis and post-synthesis methods, along with resulting relaxivities. From [68].

1.4 APPLICATIONS IN IMAGING AND DIAGNOSTICS

1.4.1 *In vitro diagnostics with silica nanoparticles*

Nanoparticles have been widely used as labels in diagnostic and imaging applications as they possess high specific activity, and even single binding events can be observed due to the extremely intense e.g. photoluminescence signal of the particles as compared to molecular labels. The higher the signal, the easier and more sensitive the detection will be. This is mainly due to a high concentration of label units within a

nanoparticle, novel particle materials or high absorption cross-section. In solid silica particles, the label content may exceed 20% (w/w) amplifying the signal from one binding reaction when compared with organic fluorophores. Furthermore, the nanoparticle shell provides protection for the fluorophore, reducing both dynamic quenching and probability of reactions leading to irreversible photobleaching [11]. In many cases, this outcome is achieved simply by excluding oxygen and water molecules from the vicinity of the fluorophore [66].

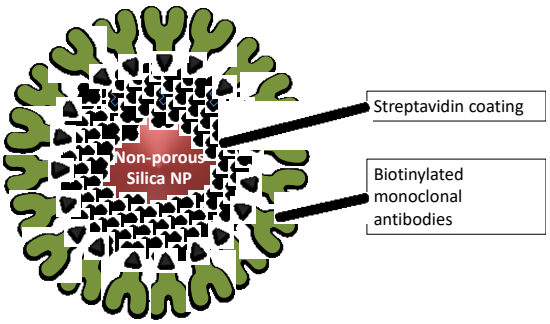

Figure 15. Schematic representation of bioconjugation where a non-porous silica NP is first coated with streptavidin and immediately prior to assay biotinylated antibodies are added to the particles to facilitate specific detection of antigens.

These particles may subsequently be coated with bioactive molecules such as antibodies and used in immunoassays or imaging, and on the labeled NPs there is a large surface area available for accommodating the bioactive molecules. To achieve efficient coating, there are various technologies ranging from nonspecific physical adsorption, elaborate bioconjugate chemistry to site-specific bioconjugation of antibody fragments and over to use of adaptor proteins, e.g. avidins, reviewed in [70]. The amount of molecules depends on the particle surface area and biomolecule size, e.g. in the case of antibodies approximately one hundred active binding sites may be achieved on a (non-porous) 60 nm NP. This in turn will make use of avidity of the binders and improve the observed overall affinity of the label higher than that of a labeled single binder. Furthermore, the large surface-to-volume ratio allows a part of the surface to be exchanged to another bioactive molecule to facilitate e.g. electrochemical detection. Printed electronics offer cost-effective means of

detection, but would often benefit from amplified signals. By utilizing HRP-antibody double coated particles, a 30-fold amplification of electrochemical signal has been obtained [71].

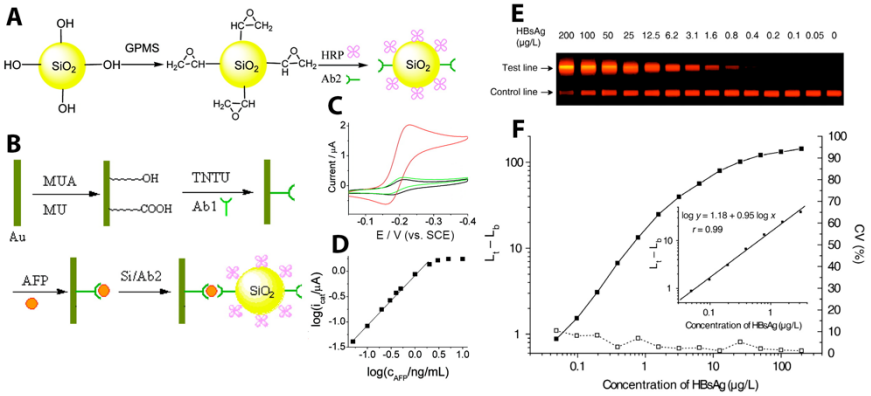

Figure 16. ***In vitro*** **diagnostics applications using non-porous silica NPs.** (A) The NPs are double functionalized with HRP and antibodies. (B) The work electrode is coated with another antibody and subsequently sample is added and then the NPs. (C) Finally, cyclic voltammogram is recorded in the presence of thioene and H_2O_2. (D) Concentration of the analyte is plotted against electrocatalytic current. (F) Eu (III) nanoparticle-based LFIA of HBsAg, calibrator images of test strips (membrane area) and a negative control in assay buffer. (E), Calibration curves (▪) and imprecision profiles (□) of panel A. The inset illustrates the linear range region of the plot. Mean value of test line luminosity (Lt) and background luminosity (Lb). Adapted from [52,71]

However, hydrolysis of silica will limit the coating strategies to some extent as high pH may not be used, and additionally, the coated bioactive nanoparticles cannot be stored for long periods of time, because the optimal storage conditions for proteins e.g. antibodies and silica NPs are different. For these reasons, the more stable non-porous silica NPs are predominantly used in diagnostic applications along with a coating on the NPs with a stabile adaptor protein e.g. streptavidin. This will facilitate storage times of several weeks for the bioactive silica NPs [72].

1.4.2 *Silica nanoparticles in live cell imaging*

Positively charged silica NPs are readily taken up by various cell types. This property has been utilized in many studies to detect and stain cells with inherently stained particles or with particles loaded with fluorescent molecules. The most common method to functionalize silica NPs with APTES and subsequently conjugate the formed primary amino groups with FITC, thus facilitating convenient tracking of the stained cells [33]. The dissolution of silica NPs is considerably slowed down by the confined (and acidic) intracellular environment. In dividing cells, the particles are diluted evenly amongst the daughter cells and decay of the signal depends on the degradation or exocytosis of the particles, amount divisions that dilute the particles and amount of dye attached to the particles. For MSNs, typical dye loadings achieved by conjugation (attachment) amount to a maximum of a couple of wt%, while adsorption strategies can yield loading degrees up to 50 wt%. The loss of signal due to dilution between daughter cells may be circumvented by this strategy, i.e. loading the particles with a dye that is released from the particles in a sustained manner over time [32]. In addition to labeling and tracking of entire cells, silica NPs allow more elaborate mechanistical studies on intracellular membrane trafficking that was able to demonstrate cargo dependent motility of endosomes [73].

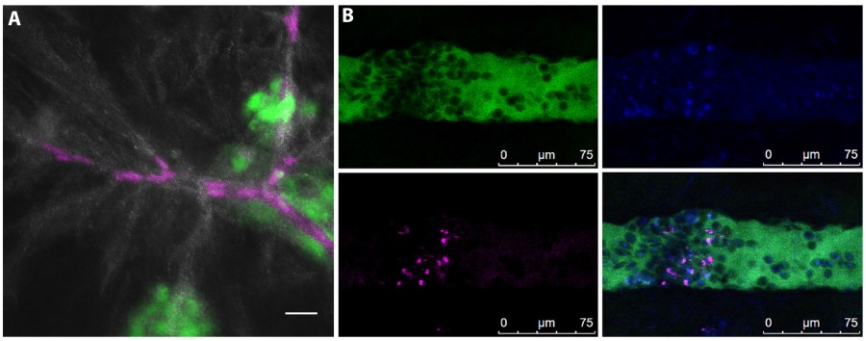

Figure 17. Tracking of cells labelled with fluorescent MSNs. A) A coculture of fibroblasts labeled with MSNs (magenta) and LNCaP cells (green), collagen is shown in white. Scale bar 30 um. B) Two-photon imaging of injected MSN stained cancer cells (magenta) circulating in CAM-model, blood pool (green) stained with dextran conjugated dye and nuclei stained with Hoechst.

1.5 CORE@SHELL NANOPARTICLES FOR MULTIMODAL IMAGING AND THERANOSTICS

The most prominent advantage of silica as a construct in the design of any nanostructure is, as already established, its synthetic flexibility. Silica can be constructed as part of nanocomposites (inorganic-inorganic) or hybrid (inorganic-organic) materials, in porous or non-porous form, and in varying morphologies (most often nanoparticles or coatings in the case of nanostructures). Since silica is not inherently detectable, its function as construct in nanostructured imaging agents is either to add functionality to the system or act as a barrier to separate two other material constructs, or protecting another construct from the surroundings. The former can be exemplified by introducing pores to a nanosystem, that can subsequently be loaded with active molecules (drugs, molecular imaging agents…) or simply maximizing the available surface area for further surface functionalization [74]. A typical example of the latter would be separating a magnetic core from a surface layer of fluorescent dyes with a silica layer, as direct contact between the dye and the magnetic NP would lead to quenching of the dye fluorescence. Other barrier functions may include protection of the core material from water (e.g. UCNPs) which would lead to luminescence quenching, or from the surrounding pH conditions that could lead to corrosion or dissolution of the core material (e.g. SPIONs). In all cases, a silica surface (porous or non-porous) provides the nanosystem with good water dispersability (hydrophilicity), enhanced colloidal stability, easy further functionalization *via* all techniques developed for silica surfaces, chemical inertness and biocompatibility. In this section, we will thus concentrate on such structures where silica is used as coating material, i.e. core@shell structures. This is perhaps the most flexible approach for constructing either multimodal or thernaostic agents, as the two or more imaging modalities and/or imaging and therapeutic functions can be distinctly separated, if the core is responsible for one function and the shell of another. There are surely multiple examples also of constructs where both active entities are molecular agents, e.g. where one is loaded into the core material, which can be porous or non-porous silica; and a second e.g. imaging agent is attached to the particle surface. From a functionality point of view, also these constructs can be regarded core@shell materials, but we will here concentrate on the physical core@shell constructs where the core and the shell are of different materials, and thus represent different functionalities.

1.5.1 *Multimodal imaging*

The rationale for multimodal imaging is gaining complementary information in "one shot" via more than one imaging technique or to approximately localize stained cells with a non-invasive method prior to a closer more detailed examination. Every imaging modality has advantages and disadvantages, and are thus highly complementary. For instance, whereas optical imaging reveals pathologies at the cellular or sub-cellular level, MRI generally display physiological differences at the level of tissues and organs [69]. This combination, optical imaging (OI) with MRI is consequently also the perhaps most common combination for the construction of bimodal imaging agents. The most typical example of a core@shell construct of this type is a magnetic core surrounded by a shell carrying fluorescent molecular dyes. As mentioned above, a solid silica shell can be used here as barrier layer to separate these, while a porous silica shell can be coated to maximize the amount of dyes that can be carried (**Figure 18**) [74].

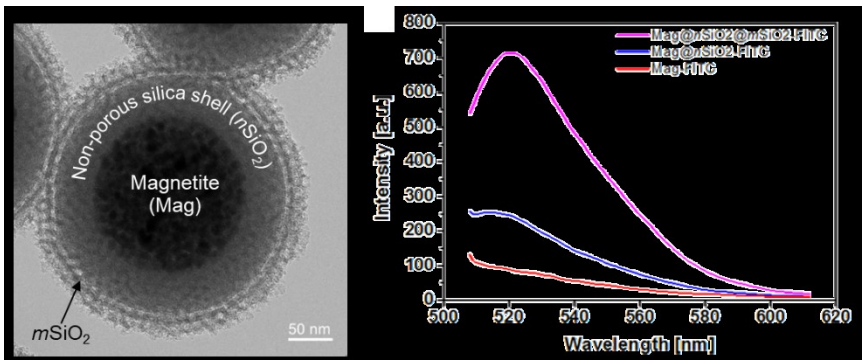

Figure 18. Core@shell@shell (Mag@nSiO$_2$@mSiO$_2$) constructs consisting of a superparamagnetic iron oxide core (Mag) and a non-porous silica inner shell (nSiO$_2$) separating the core from the mesoporous silica outer shell (mSiO$_2$). The TEM image shows the morphology and structure of the construct while the fluorescence intensity measurements show the impact of the barrier layer on the fluorescence of attached dyes (FITC). The porous outer layer allows maximization of the amount dye molecules that can be attached to the nanosystem.

As outlined in section *1.3.1. Silica nanoparticles as carriers for optical imaging agents*, maximizing the amount of dyes in the shell does not necessarily correspond to the highest imaging signal (in this case, intensity). The same holds true for the core material; an imaging signal originating from the

activity of the core NP will most likely be altered upon coating of a shell. Non-porous coatings are commonly used to protect core NPs from surrounding water if water contact may lead to luminescence quenching, as is the case for UCNPs [37]. However, when porous coatings are considered, the pores are most often radially aligned within the shell, which means that water still has direct access to the core material. In the case of magnetic cores, such as iron oxides intended for use as contrast agents for MR-imaging, the presence of a porous shell has actually shown to quite drastically enhance the relaxometric properties of the core. Primarily, the properties of the magnetic core material itself, including magnetic parameters (magnetic susceptibility (χ), saturation magnetization (m_s), anisotropy (K), Néel relaxation time (τ_N), Brownian relaxation time (τ_B)) and surface functionalities of the magnetic NPs can be tuned via the magnetic NP size, composition, and surface chemistry [75]. Additionally, not only the presence of a coating but further, the properties of the coating material will further alter the relaxivity of the resulting NP system. In the case of porous silica coatings, it is mainly the pore size of the shell that will have a profound impact on the resultant relaxivity (**Figure 19**).

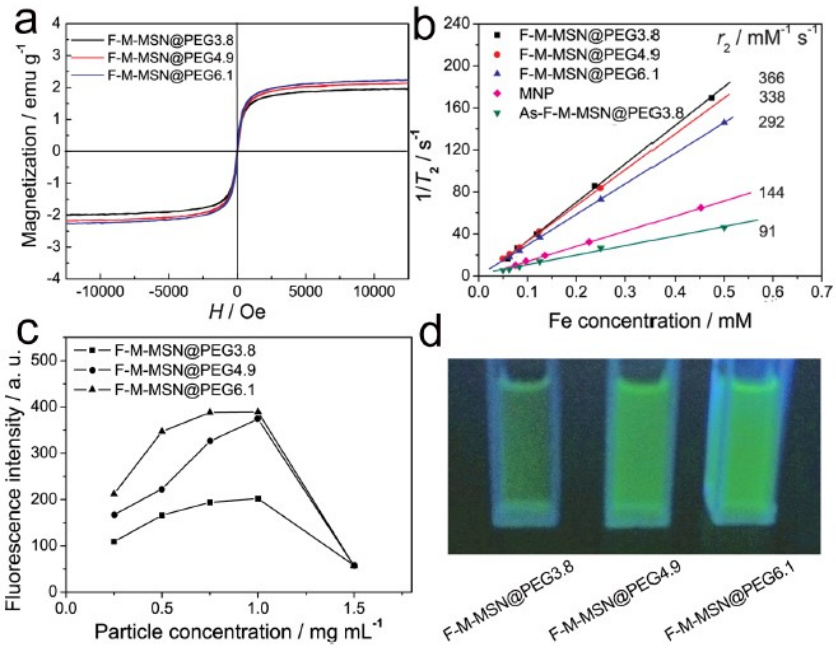

Figure 19. Pore size dependence on relaxivity. a) Field-dependent magnetization curves at 300 K. An enlargement of the central part of the curves is shown in the inset. b) T_2 relaxivity (r_2) plots for the aqueous suspensions of F-M-MSN@PEG with different pore sizes, the slopes indicate r_2. c) Peak fluorescence emission as a function of the particle concentration. d) The photograph of F-M-MSN@PEG suspensions (0.5 mg mL−1) irradiated with UV light.

As seen in Fig. 18, the highest relaxivity was obtained with the smallest pore size of 3.8 nm, while the relaxivity markedly decreased with increasing pore size. This can be understood, as the diffusion of water in mesopores slows down with a decrease in the pore size [76], a longer confinement effect and thus, residence time can be achieved for the protons in smaller mesopores, prolonging their interaction within the magnetic NP-generated local magnetic fields leading to enhanced relaxivity [77]. Notably, for the non-extracted sample i.e. pores not liberated from the template yet, thus resembling that of a non-porous coating, the relaxivity is less than that for the pure iron oxide core. Further observable in the figure, is that the fluorescence of the fluorescent dyes

conjugated inside the mesopores follow the opposite trend. Here, an enlarged pore size provides for enhanced fluorescence due to less self-quenching processes taking place in the confined space of the mesopores (as discussed in section 1.3.1.). From this demonstration follows that the design should be judiciously chosen depending on the foreseen application. Given the flexibility of the silica coating procedures, virtually any core material can be chosen for a core@shell design encompassing a porous layer. This opens up for the possibilities of constructing core@shell material from optically active cores (QD, UCNP, ND) with porous shells, while also the optical properties of the cores may be affected by the coating [78]. Both porous and non-porous silica coatings can further be utilized for the attachment of paramagnetic complexes, doping of ions f or MR-imaging or radiolabeling via chelator-based or chelator-free methods for PET imaging [79]. There are also a few examples of using silica NPs as agents for ultrasound (US) imaging, e.g. superhydrophobic MSNs exhibited a significant and strong US contrast intensity compared with other nanoparticles by enhanced stabilization of microbubbles [80]. Based on these modularities, a multitude of complex architectures can be found in the literature, and there are several comprehensive reviews that has covered these lately that the interested reader is kindly referred to, e.g. the following ones: [5,17,81]

1.5.2 Intracellular sensing

Silica NP based optical pH sensors coupled with photoluminescent indicator dyes facilitate measurements without a direct contact or perturbing the observed system. Here as well, the use of bright fluorescent silica NPs enables sensitive detection and precise localization [85]. The probes can be miniaturized to the size of intracellular organelles, readily internalized in living cells and even be used for *in vivo* imaging. The luminescent pH indicators have a dynamic range of 3–4 pH units that usually covers the range of pH changes in living systems. A crucial aspect that may be achieved with silica NPs is referencing of the sensor signals to ascertain that changes in the intensity are not caused by local changes in probe concentration. Moreover, the core@shell strategy may be employed to detect multiple parameters from intracellular milieu like in simultaneous detection of dissolved oxygen and pH [86].

1.5.3 Theranostic prospects

The most exploited designs for core@shell structures involving a porous shell are nevertheless not multimodal imaging probes, but prospective theranostic agents. In this context, 'theranostic agents' refer to nanosystems capable of both imaging (diagnostics) and drug delivery (therapy). The obvious division of labor is the core material catering for the imaging modality, while the porous shell functions as drug carrier. Taken into account that the porous shell in itself influences the imaging signal, it is palpable that the loading of drug molecules into the porous layer surrounding the core material will have an impact on the same. This has, however, not been well investigated in the literature but rather a multitude of different design combinations can be found, which are too vast to cover here. Nevertheless, all of the above-discussed design aspects can be utilized and combined in different ways to create a multifunctional nanosystem encompassing both diagnostic and therapeutic capabilities. Furthermore, other types of advantages can be exploited based on the properties of the individual constructs, such as magnetic targeting and/or magnetically enhanced cell uptake in the case of magnetic nanocomposites (**Figure 20**). Certain materials inherently encompass properties rendering them useful for therapy in themselves, such as photodynamic and photothermal therapy, or hyperthermia (magnetic NPs) that could be further combined with the delivery of drugs [82].

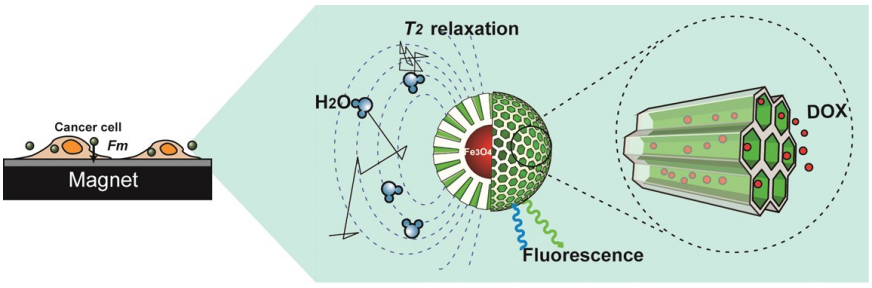

Figure 20. Schematic representation of triple-functional M-MSNs. The nanocomposite has a Fe_3O_4 nanocrystal core coated with a mesoporous silica shell doped with FITC, and can enhance the proton *T*2 relaxation in water. The cellular uptake of M-MSNs was enhanced by the magnetic field. With large pore volumes, the nanoparticles could be used for magnetic delivery of anticancer drugs [83].

The main advantage obtained by the integration of a diagnostic functionality into a drug delivery system is still most likely for promoting the development of nanotherapeutics in enabling monitoring of the drug delivery process, as well as following the individual's therapeutic response. This not only enables patient pre-selection of the individuals that are most likely to respond well to the therapy, but also aids in putting forward the nanotherapeutics with the highest clinical translatability [84]. Despite the high hopes devoted to nanomedicines especially in cancer therapy, and the substantial research efforts that have been directed towards the development of methods to improve site-specific delivery of chemotherapeutics, this largely still remains an unattainable goal [5]. Here, imaging can play a crucial role in the discovery of more successful methods for studying the targeting efficiency in order to improve the specificity of nanotherapeutic delivery. Further, imaging promotes the understanding the interactions between nanomaterials and biological systems, i.e. the "nano-bio interface". These aspects constitute where "nanotheranostics" is anticipated to be of critical importance toward the development of personalized medicines and improved efficacy and safety of nanomedicine-based therapies.

1.6 CONCLUSIONS

Silica has indeed been proven to be a highly flexible material with regard to modular and flexible design options, and a range of advantageous properties that can be utilized in bioimaging and other biomedical applications. Nevertheless, the conceptual demonstrations illustrated here is to show that each novel construction of imaging agents should indeed follow a rational design approach, as the interdependencies of the properties of the constructs may be multiple. For multimodal imaging probes, the situation becomes even more complex, when the dependency of several imaging modalities need to be taken into account and the dependencies are seldom linear (such as concentration dependent) as in the case of both luminescence and MRI, as have been demonstrated with several examples throughout this chapter. A multitude of designs exist in the literature, with recent emphasis on multifunctional and theranostic systems. The greatest benefit of these nanoscopic imaging, diagnostic or

theranostic agents will most likely be the information that can be gained through imaging for promoting the development of new nanotherapeutic systems. Eventually, multifunctional and/or multimodal imagining agents could aid in generating a new generation of nanotherapeutics with improved specificity, efficacy and safety.

References

1 Kuhlmann, A. M. (1963) The Second Most Abundant Element in the Earth's Crust. JOM **15**, 502–505.
2 (2013) Handbook of Pharmaceutical Excipients – 7th Edition. Pharm. Dev. Technol. **18**, 544–544.
3 Hench, L. L. and Jones, J. R. (2015) Bioactive Glasses: Frontiers and Challenges. Front. Bioeng. Biotechnol. **3**.
4 Unger, K., Rupprecht, H., Valentin, B. and Kircher, W. (1983) The use of porous and surface modified silicas as drug delivery and stabilizing agents. Drug Dev. Ind. Pharm. **9**, 69–91.
5 Karaman, D. Ş., Sarparanta, M. P., Rosenholm, J. M. and Airaksinen, A. J. Multimodality Imaging of Silica and Silicon Materials In Vivo. Adv. Mater. **0**, 1703651.
6 Burns, A., Ow, H. and Wiesner, U. (2006) Fluorescent core–shell silica nanoparticles: towards "Lab on a Particle" architectures for nanobiotechnology. Chem. Soc. Rev. **35**, 1028–1042.
7 Iler, R. K. (1979) The Chemistry of Silica: Solubility, Polymerization, Colloid and Surface Properties and Biochemistry of Silica, Wiley.
8 Stöber, W., Fink, A. and Bohn, E. (1968) Controlled growth of monodisperse silica spheres in the micron size range. J. Colloid Interface Sci. **26**, 62–69.
9 Kolbe, G. (1956) Das komplexchemische Verhalten der Kieselsäure.
10 Bazuła, P. A., Arnal, P. M., Galeano, C., Zibrowius, B., Schmidt, W. and Schüth, F. (2014) Highly microporous monodisperse silica spheres synthesized by the Stöber process. Microporous Mesoporous Mater. **200**, 317–325.
11 Auger, A., Samuel, J., Poncelet, O. and Raccurt, O. (2011) A comparative study of non-covalent encapsulation methods for organic dyes into silica nanoparticles. Nanoscale Res. Lett. **6**, 328.
12 Xu, Z., Ma, X., Gao, Y.-E., Hou, M., Xue, P., Li, C. M. and Kang, Y. (2017) Multifunctional silica nanoparticles as a promising theranostic platform for biomedical applications. Mater. Chem. Front. **1**, 1257–1272.
13 Osseo-Asare, null and Arriagada, null. (1999) Growth Kinetics of Nanosize Silica in a Nonionic Water-in-Oil Microemulsion: A Reverse Micellar Pseudophase Reaction Model. J. Colloid Interface Sci. **218**, 68–76.
14 Tavernaro, I., Cavelius, C., Peuschel, H. and Kraegeloh, A. (2017) Bright fluorescent silica-nanoparticle probes for high-resolution STED and confocal microscopy. Beilstein J. Nanotechnol. **8**, 1283–1296.
15 Yoo, H. and Pak, J. (2013) Synthesis of highly fluorescent silica nanoparticles in a reverse microemulsion through double-layered doping of organic fluorophores. J. Nanoparticle Res. **15**, 1609.
16 Mahon, E., Hristov, D. R. and Dawson, K. A. (2012) Stabilising fluorescent silica

nanoparticles against dissolution effects for biological studies. Chem. Commun. **48**, 7970–7972.
17 Shirshahi, V. and Soltani, M. (2015) Solid silica nanoparticles: applications in molecular imaging. Contrast Media Mol. Imaging **10**, 1–17.
18 Ow, H., Larson, D. R., Srivastava, M., Baird, B. A., Webb, W. W. and Wiesner, U. (2005) Bright and Stable Core−Shell Fluorescent Silica Nanoparticles. Nano Lett. **5**, 113–117.
19 Larson, D. R., Ow, H., Vishwasrao, H. D., Heikal, A. A., Wiesner, U. and Webb, W. W. (2008) Silica Nanoparticle Architecture Determines Radiative Properties of Encapsulated Fluorophores. Chem. Mater. **20**, 2677–2684.
20 Yao, G., Wang, L., Wu, Y., Smith, J., Xu, J., Zhao, W., Lee, E. and Tan, W. (2006) FloDots: luminescent nanoparticles. Anal. Bioanal. Chem. **385**, 518–524.
21 Das, S., Jain, T. K. and Maitra, A. (2002) Inorganic-organic hybrid nanoparticles from n-octyl triethoxy silane. J. Colloid Interface Sci. **252**, 82–88.
22 Sharma, R. K., Das, S. and Maitra, A. (2004) Surface modified ormosil nanoparticles. J. Colloid Interface Sci. **277**, 342–346.
23 Yanagisawa, T., Shimizu, T., Kuroda, K. and Kato, C. (1990) The Preparation of Alkyltriinethylaininonium–Kaneinite Complexes and Their Conversion to Microporous Materials. Bull. Chem. Soc. Jpn. **63**, 988–992.
24 Beck, J. S., Vartuli, J. C., Roth, W. J., Leonowicz, M. E., Kresge, C. T., Schmitt, K. D., Chu, C. T. W., Olson, D. H., Sheppard, E. W., McCullen, S. B., et al. (1992) A new family of mesoporous molecular sieves prepared with liquid crystal templates. J. Am. Chem. Soc. **114**, 10834–10843.
25 Kresge, C. T., Leonowicz, M. E., Roth, W. J., Vartuli, J. C. and Beck, J. S. (1992) Ordered mesoporous molecular sieves synthesized by a liquid-crystal template mechanism. Nature **359**, 710–712.
26 Liu, J., Kim, A. Y., Wang, L. Q., Palmer, B. J., Chen, Y. L., Bruinsma, P., Bunker, B. C., Exarhos, G. J., Graff, G. L., Rieke, P. C., et al. (1996) Self-assembly in the synthesis of ceramic materials and composites. Adv. Colloid Interface Sci. **69**, 131–180.
27 Meynen, V., Cool, P. and Vansant, E. F. (2009) Verified syntheses of mesoporous materials. Microporous Mesoporous Mater. **125**, 170–223.
28 M. Rosenholm, J., Sahlgren, C. and Lindén, M. (2010) Towards multifunctional, targeted drug delivery systems using mesoporous silica nanoparticles – opportunities & challenges. Nanoscale **2**, 1870–1883.
29 Maleki, A., Kettiger, H., Schoubben, A., Rosenholm, J. M., Ambrogi, V. and Hamidi, M. (2017) Mesoporous silica materials: From physico-chemical properties to enhanced dissolution of poorly water-soluble drugs. J. Controlled Release **262**, 329–347.
30 Gomes, M. C., Cunha, Â., Trindade, T. and Tomé, J. P. C. (2016) The role of surface functionalization of silica nanoparticles for bioimaging. J. Innov. Opt. Health Sci. **09**, 1630005.
31 Hoffmann Frank, Cornelius Maximilian, Morell Jürgen and Fröba Michael. (2006) Silica-Based Mesoporous Organic–Inorganic Hybrid Materials. Angew. Chem. Int. Ed. **45**, 3216–3251.
32 Rosenholm, J. M., Gulin-Sarfraz, T., Mamaeva, V., Niemi, R., Özliseli, E., Desai, D., Antfolk, D., von Haartman, E., Lindberg, D., Prabhakar, N., et al. (2016) Prolonged Dye Release from Mesoporous Silica-Based Imaging Probes Facilitates Long-Term Optical Tracking of Cell Populations In Vivo. Small Weinh. Bergstr. Ger. **12**, 1578–1592.
33 Karaman, D. S., Desai, D., Senthilkumar, R., Johansson, E. M., Råtts, N., Odén, M., Eriksson, J. E., Sahlgren, C., Toivola, D. M. and Rosenholm, J. M. (2012) Shape engineering vs organic modification of inorganic nanoparticles as a tool for enhancing cellular internalization. Nanoscale Res. Lett. **7**, 358.

34 Prabhakar, N., Näreoja, T., von Haartman, E., Karaman, D. Ş., Jiang, H., Koho, S., Dolenko, T. A., Hänninen, P. E., Vlasov, D. I., Ralchenko, V. G., et al. (2013) Core-shell designs of photoluminescent nanodiamonds with porous silica coatings for bioimaging and drug delivery II: application. Nanoscale **5**, 3713–3722.
35 Desai, D., Karaman, D. S., Prabhakar, N., Tadayon, S., Duchanoy, A., Toivola, D. M., Rajput, S., Näreoja, T. and Rosenholm, J. M. (2014) Design considerations for mesoporous silica nanoparticulate systems in facilitating biomedical applications. Mesoporous Biomater. **1**.
36 Ghosh Chaudhuri, R. and Paria, S. (2012) Core/Shell Nanoparticles: Classes, Properties, Synthesis Mechanisms, Characterization, and Applications. Chem. Rev. **112**, 2373–2433.
37 Liu, D., Xu, X., Wang, F., Zhou, J., Mi, C., Zhang, L., Lu, Y., Ma, C., Goldys, E., Lin, J., et al. (2016) Emission stability and reversibility of upconversion nanocrystals. J. Mater. Chem. C **4**, 9227–9234.
38 Duan, C., Liang, L., Li, L., Zhang, R. and Xu, Z. P. (2018) Recent progress in upconversion luminescence nanomaterials for biomedical applications. J. Mater. Chem. B **6**, 192–209.
39 Chen, Y.-S., Frey, W., Kim, S., Homan, K., Kruizinga, P., Sokolov, K. and Emelianov, S. (2010) Enhanced thermal stability of silica-coated gold nanorods for photoacoustic imaging and image-guided therapy. Opt. Express **18**, 8867–8878.
40 Alwi, R., Telenkov, S., Mandelis, A., Leshuk, T., Gu, F., Oladepo, S. and Michaelian, K. (2012) Silica-coated super paramagnetic iron oxide nanoparticles (SPION) as biocompatible contrast agent in biomedical photoacoustics. Biomed. Opt. Express **3**, 2500–2509.
41 Wu, W., Wu, Z., Yu, T., Jiang, C. and Kim, W.-S. (2015) Recent progress on magnetic iron oxide nanoparticles: synthesis, surface functional strategies and biomedical applications. Sci. Technol. Adv. Mater. **16**, 023501.
42 Bumb, A., Sarkar, S. K., Billington, N., Brechbiel, M. W. and Neuman, K. C. (2013) Silica Encapsulation of Fluorescent Nanodiamonds for Colloidal Stability and Facile Surface Functionalization. J. Am. Chem. Soc. **135**, 7815–7818.
43 Kim, J., Lee, J. E., Lee, J., Yu, J. H., Kim, B. C., An, K., Hwang, Y., Shin, C.-H., Park, J.-G., Kim, J., et al. (2006) Magnetic Fluorescent Delivery Vehicle Using Uniform Mesoporous Silica Spheres Embedded with Monodisperse Magnetic and Semiconductor Nanocrystals. J. Am. Chem. Soc. **128**, 688–689.
44 Nooney, R. I., Thirunavukkarasu, D., Chen, Y., Josephs, R. and Ostafin, A. E. (2003) Self-Assembly of Mesoporous Nanoscale Silica/Gold Composites. Langmuir **19**, 7628–7637.
45 Cai, Q., Luo, Z.-S., Pang, W.-Q., Fan, Y.-W., Chen, X.-H. and Cui, F.-Z. (2001) Dilute Solution Routes to Various Controllable Morphologies of MCM-41 Silica with a Basic Medium. Chem. Mater. **13**, 258–263.
46 Zhang, J., Li, X., Rosenholm, J. M. and Gu, H. (2011) Synthesis and characterization of pore size-tunable magnetic mesoporous silica nanoparticles. J. Colloid Interface Sci. **361**, 16–24.
47 Kim, T., Momin, E., Choi, J., Yuan, K., Zaidi, H., Kim, J., Park, M., Lee, N., McMahon, M. T., Quinones-Hinojosa, A., et al. (2011) Mesoporous Silica-Coated Hollow Manganese Oxide Nanoparticles as Positive T1 Contrast Agents for Labeling and MRI Tracking of Adipose-Derived Mesenchymal Stem Cells. J. Am. Chem. Soc. **133**, 2955–2961.
48 Chen, J., Zhang, R., Han, L., Tu, B. and Zhao, D. (2013) One-pot synthesis of thermally stable gold@mesoporous silica core-shell nanospheres with catalytic activity. Nano Res. **6**, 871–879.
49 Nelson, D. K., Razbirin, B. S., Starukhin, A. N., Eurov, D. A., Kurdyukov, D. A.,

Stovpiaga, E. Y. and Golubev, V. G. (2016) Photoluminescence of carbon dots from mesoporous silica. Opt. Mater. **59**, 28–33.
50 Jiao, J., Liu, C., Li, X., Liu, J., Di, D., Zhang, Y., Zhao, Q. and Wang, S. (2016) Fluorescent carbon dot modified mesoporous silica nanocarriers for redox-responsive controlled drug delivery and bioimaging. J. Colloid Interface Sci. **483**, 343–352.
51 Hai, X., Tan, M., Wang, G., Ye, Z., Yuan, J. and Matsumoto, K. (2004) Preparation and a Time-Resolved Fluoroimmunoassay Application of New Europium Fluorescent Nanoparticles. Anal. Sci. **20**, 245–246.
52 Xia, X., Xu, Y., Zhao, X. and Li, Q. (2009) Lateral Flow Immunoassay Using Europium Chelate-Loaded Silica Nanoparticles as Labels. Clin. Chem. **55**, 179–182.
53 Rosenholm, J. M., Czuryszkiewicz, T., Kleitz, F., Rosenholm, J. B. and Lindén, M. (2007) On the Nature of the Brønsted Acidic Groups on Native and Functionalized Mesoporous Siliceous SBA-15 as Studied by Benzylamine Adsorption from Solution. Langmuir **23**, 4315–4323.
54 Valetti, S., Feiler, A. and Trulsson, M. (2017) Bare and Effective Charge of Mesoporous Silica Particles. Langmuir ACS J. Surf. Colloids **33**, 7343–7351.
55 Gulin-Sarfraz, T., Sarfraz, J., Karaman, D. Ş., Zhang, J., Oetken-Lindholm, C., Duchanoy, A., Rosenholm, J. M. and Abankwa, D. (2014) FRET-reporter nanoparticles to monitor redox-induced intracellular delivery of active compounds. RSC Adv. **4**, 16429–16437.
56 von Haartman, E., Lindberg, D., Prabhakar, N. and Rosenholm, J. M. (2016) On the intracellular release mechanism of hydrophobic cargo and its relation to the biodegradation behavior of mesoporous silica nanocarriers. Eur. J. Pharm. Sci. **95**, 17–27.
57 Bérubé, F., Khadraoui, A., Florek, J., Kaliaguine, S. and Kleitz, F. (2015) A generalized method toward high dispersion of transition metals in large pore mesoporous metal oxide/silica hybrids. J. Colloid Interface Sci. **449**, 102–114.
58 Kim, S. M., Im, G. H., Lee, D.-G., Lee, J. H., Lee, W. J. and Lee, I. S. (2013) Mn2+-doped silica nanoparticles for hepatocyte-targeted detection of liver cancer in T1-weighted MRI. Biomaterials **34**, 8941–8948.
59 Sarparanta, M. (2013) 18F-Radiolabeled porous silicon particles for drug delivery : Tracer development and evaluation in rats.
60 Sarparanta, M., Mäkilä, E., Heikkilä, T., Salonen, J., Kukk, E., Lehto, V.-P., Santos, H. A., Hirvonen, J. and Airaksinen, A. J. (2011) 18F-Labeled Modified Porous Silicon Particles for Investigation of Drug Delivery Carrier Distribution in Vivo with Positron Emission Tomography. Mol. Pharm. **8**, 1799–1806.
61 Carniato, F., Tei, L., Arrais, A., Marchese, L. and Botta, M. (2013) Selective Anchoring of GdIII Chelates on the External Surface of Organo-Modified Mesoporous Silica Nanoparticles: A New Chemical Strategy To Enhance Relaxivity. Chem. – Eur. J. **19**, 1421–1428.
62 Taylor-Pashow, K. M. L., Rocca, J. D. and Lin, W. (2011) Mesoporous Silica Nanoparticles with Co-Condensed Gadolinium Chelates for Multimodal Imaging. Nanomaterials **2**, 1–14.
63 Davis, J. J., Huang, W.-Y. and Davies, G.-L. (2012) Location-tuned relaxivity in Gd-doped mesoporous silica nanoparticles. J. Mater. Chem. **22**, 22848–22850.
64 Laprise-Pelletier, M., Bouchoucha, M., Lagueux, J., Chevallier, P., Lecomte, R., Gossuin, Y., Kleitz, F. and Fortin, M.-A. (2015) Metal chelate grafting at the surface of mesoporous silica nanoparticles (MSNs): physico-chemical and biomedical imaging assessment. J. Mater. Chem. B **3**, 748–758.
65 Li, Y.-J. and Yan, B. (2009) Lanthanide (Eu3+, Tb3+)/β-Diketone Modified Mesoporous

SBA-15/Organic Polymer Hybrids: Chemically Bonded Construction, Physical Characterization, and Photophysical Properties. Inorg. Chem. **48**, 8276–8285.
66 Zhang, J., Prabhakar, N., Näreoja, T. and Rosenholm, J. M. (2014) Semiconducting Polymer Encapsulated Mesoporous Silica Particles with Conjugated Europium Complexes: Toward Enhanced Luminescence under Aqueous Conditions. ACS Appl. Mater. Interfaces **6**, 19064–19074.
67 Guillet-Nicolas, R., Bridot, J.-L., Seo, Y., Fortin, M.-A. and Kleitz, F. (2011) Enhanced Relaxometric Properties of MRI "Positive" Contrast Agents Confined in Three-Dimensional Cubic Mesoporous Silica Nanoparticles. Adv. Funct. Mater. **21**, 4653–4662.
68 Karaman, D. Ş., Desai, D., Zhang, J., Tadayon, S., Unal, G., Teuho, J., Sarfraz, J., Smått, J.-H., Gu, H., Näreoja, T., et al. (2016) Modulation of the structural properties of mesoporous silica nanoparticles to enhance the T1-weighted MR imaging capability. J. Mater. Chem. B **4**, 1720–1732.
69 Verwilst, P., Park, S., Yoon, B. and Kim, J. S. (2015) Recent advances in Gd-chelate based bimodal optical/MRI contrast agents. Chem. Soc. Rev. **44**, 1791–1806.
70 Sapsford, K. E., Algar, W. R., Berti, L., Gemmill, K. B., Casey, B. J., Oh, E., Stewart, M. H. and Medintz, I. L. (2013) Functionalizing Nanoparticles with Biological Molecules: Developing Chemistries that Facilitate Nanotechnology. Chem. Rev. **113**, 1904–2074.
71 Wu, Y., Chen, C. and Liu, S. (2009) Enzyme-Functionalized Silica Nanoparticles as Sensitive Labels in Biosensing. Anal. Chem. **81**, 1600–1607.
72 J. Moore, C., Montón, H., O'Kennedy, R., E. Williams, D., Nogués, C., Lynam), C. C. (née and Gubala, V. (2015) Controlling colloidal stability of silica nanoparticles during bioconjugation reactions with proteins and improving their longer-term stability, handling and storage. J. Mater. Chem. B **3**, 2043–2055.
73 Aoyama, M., Yoshioka, Y., Arai, Y., Hirai, H., Ishimoto, R., Nagano, K., Higashisaka, K., Nagai, T. and Tsutsumi, Y. (2017) Intracellular trafficking of particles inside endosomal vesicles is regulated by particle size. J. Controlled Release **260**, 183–193.
74 Gulin-Sarfraz, T., Zhang, J., Desai, D., Teuho, J., Sarfraz, J., Jiang, H., Zhang, C., Sahlgren, C., Lindén, M., Gu, H., et al. (2014) Combination of magnetic field and surface functionalization for reaching synergistic effects in cellular labeling by magnetic core–shell nanospheres. Biomater. Sci. **2**, 1750–1760.
75 Shin, T.-H., Choi, Y., Kim, S. and Cheon, J. (2015) Recent advances in magnetic nanoparticle-based multi-modal imaging. Chem. Soc. Rev. **44**, 4501–4516.
76 Walther Hansen, E., Schmidt, R., Stöcker, M. and Akporiaye, D. (1995) Self-diffusion coefficient of water confined in mesoporous MCM-41 materials determined by 1H nuclear magnetic resonance spin-echo measurements. Microporous Mater. **5**, 143–150.
77 Zhang, J., Rosenholm, J. M. and Gu, H. (2012) Molecular Confinement in Fluorescent Magnetic Mesoporous Silica Nanoparticles: Effect of Pore Size on Multifunctionality. ChemPhysChem **13**, 2016–2019.
78 Liu, N. and Yang, P. (2013) Highly luminescent hybrid SiO2-coated CdTe quantum dots: synthesis and properties. Luminescence **28**, 542–550.
79 Ni, D., Jiang, D., Ehlerding, E. B., Huang, P. and Cai, W. (2018) Radiolabeling Silica-Based Nanoparticles via Coordination Chemistry: Basic Principles, Strategies, and Applications. Acc. Chem. Res. **51**, 778–788.
80 Jin, Q., Lin, C.-Y., Kang, S.-T., Chang, Y.-C., Zheng, H., Yang, C.-M. and Yeh, C.-K. (2017) Superhydrophobic silica nanoparticles as ultrasound contrast agents. Ultrason. Sonochem. **36**, 262–269.
81 Caltagirone, C., Bettoschi, A., Garau, A. and Montis, R. (2015) Silica-based nanoparticles: a versatile tool for the development of efficient imaging agents. Chem. Soc. Rev. **44**, 4645–4671.

82 Huang, H. and Lovell, J. F. (2017) Advanced Functional Nanomaterials for Theranostics. Adv. Funct. Mater. **27**, 1603524.
83 Liu, Q., Zhang, J., Xia, W. and Gu, H. (2012) Towards magnetic-enhanced cellular uptake, MRI and chemotherapeutics delivery by magnetic mesoporous silica nanoparticles. J. Nanosci. Nanotechnol. **12**, 7709–7715.
84 Arranja, A. G., Pathak, V., Lammers, T. and Shi, Y. (2017) Tumor-targeted nanomedicines for cancer theranostics. Pharmacol. Res. **115**, 87–95.
85 Burns, A., Sengupta, P., Zedayko, T., Baird, B. and Wiesner, U. (2006) Core/Shell Fluorescent Silica Nanoparticles for Chemical Sensing: Towards Single-Particle Laboratories. Small **2**, 723–726.
86 Wang, X., Stolwijk, J. A., Lang, T., Sperber, M., Meier, R. J., Wegener, J. and Wolfbeis, O. S. (2012) Ultra-Small, Highly Stable, and Sensitive Dual Nanosensors for Imaging Intracellular Oxygen and pH in Cytosol. J. Am. Chem. Soc. **134**, 17011–17014.